Technical Report

Liquid Argon for Direct Dark Matter Detection

G. Fiorillo[1,2] and G. Matteucci[1,2]

[1]*Physics Department, Università degli Studi di Napoli "Federico II", 80126 Napoli, Italy*

[2]*INFN Sezione di Napoli, 80126 Napoli, Italy*

Corresponding author: G. Fiorillo
Email address: giuseppe.matteucci@na.infn.it

Abstract

The pursuit of understanding dark matter has been fostering innovation in the field of particle detectors, simultaneously pushing the boundaries toward higher sensitivity and exposure. Liquid argon detectors, specifically time projection chambers, hold immense promise due to their capability of measuring both ionization and scintillation signals while taking advantage of the pulse-shape discrimination properties provided by argon scintillation channels. Enhancements in liquid argon purification, reduced radioactivity, and novel photodetectors will allow such detectors to be a dominant technology for next-generation experiments. These advances herald a new era in deciphering the secrets of dark matter, offering potential breakthroughs in our comprehension of the universe's composition.

Keywords: dark matter, wimp, liquid argon, underground argon, PSD, time projection chamber, TPC, LArTPC, pulse shape discrimination, SiPM, WLS, DarkSide, DEAP, ARGO, DUNE
DOI: 10.31526/JAIS.2024.523

1. DARK MATTER: UNRAVELING THE COSMIC MYSTERY

In modern cosmology and particle physics, the nature of dark matter remains unsolved. One established field of research for testing various particle hypotheses for dark matter is that of direct detection, i.e., measuring the interaction of a dark matter particle with ordinary matter in a low-background high-sensitivity detector [1]. As of today, a great number of detector technologies have already been proposed and/or implemented in experiments; however, all of them have reported results compatible with the null hypothesis, with exceptions made for a few cases still under debate. Many experiments built for the purpose of revealing dark matter, particularly those relevant to WIMP searches, can be summarized as extremely sensitive counting experiments of rare candidate signals versus background events. For such experimental communities, the major challenges associated with the next generation of direct detection experiments can be identified in an increase of the exposure to probe smaller interaction cross sections, while keeping the background rate as small as possible. These two issues, the scaling-up and the background mitigation of an experiment, comprise at their core the essence of technological advancements in the fields of engineering, applied physics, and advanced data analysis and simulations, needed to probe rarer dark matter hypothetical interactions.

In this scenario, liquid argon detectors have thoroughly demonstrated to be a powerful and effective technology, suited to overcome the mentioned challenges for the future of dark matter research. The scintillation properties of liquid argon make it a compelling choice for low-energy experiments with thresholds in the keV scale, where background is a major concern, as it provides a powerful background rejection tool from the analysis of a signal's pulse shape.

This review focuses on established and proposed technologies for dark matter direct detection with liquid argon detectors, exploring the key features, methodologies, and obstacles associated with this broad class of detectors.

1.1. WIMP Dark Matter

Given the abundance of astronomical and cosmological evidence for the existence of dark matter and its relevance in cosmic dynamics at and above the galactic scale, a diverse array of candidates has emerged as potential constituents of dark matter, spanning a wide range of properties and interaction channels with ordinary matter. Any particle candidate must have a set of properties constrained by observations: it must have zero electric charge [2], be nonbaryonic, and be stable on a cosmological time scale [3]. In addition, any candidate or set of candidates should be in accordance with the ΛCDM (Lambda Cold Dark Matter) model, the widely accepted cosmological framework that provides a comprehensive description of the universe's evolution and structure. The ΛCDM model explains a wide range of observed phenomena, including the large-scale distribution of galaxies [4], the angular anisotropies of the cosmic microwave background [5, 6], and the expansion rate of the universe. According to the ΛCDM model, dark matter is composed of particles with nonrelativistic (cold) velocities at the time of decoupling from the primordial plasma and accounts for approximately 27% of the total mass-energy content of the universe.

The WIMP (Weakly Interacting Massive Particle) hypothesis presents a compelling and naturally occurring scenario for a potential dark matter candidate, encompassing a range of stable or semistable particles that emerge from extensions to the standard

model of particle physics. In the early universe, a hypothetical dark matter particle coupled to the standard model and thermally produced would be in constant equilibrium with the surrounding plasma, with equally balanced production and annihilation processes to and from standard matter particles. As the universe expands and cools down, interactions become more and more rare, to the point of freezing out the comoving dark matter density and preserving its value to the present day. By projecting back the presently measured value of dark matter density, the thermally averaged annihilation rate can be estimated to be approximately $\langle \sigma v \rangle \approx 10^{-26}\,\mathrm{cm^3\,s^{-1}}$ [7] which falls, remarkably, in the weak interaction scale. The observation that a coupling of the same order as the weak interaction would result in the observed amount of dark matter in the universe is a substantial motivation for the existence of a particle with these properties, the WIMP. This apparent coincidence, the simplicity of the model, and the fact that WIMP particles are predicted by many natural extensions of the standard model make the WIMP a plausible and well-justified contender for the role of dark matter.

1.2. Principles of Direct Detection

Some dark matter models can be tested via the measurement of a scattering event in a terrestrial detector, with the main requirement being that of a high enough deposited energy to be within the accessible range of the detector. WIMPs have been arguably the most hunted particle, with experiments dating back to the 1980s, for both their theoretical foundation and testability with current and near-future detector technologies. The expected interaction with ordinary matter is coherent nuclear scattering that would produce a nuclear recoil of up to a few hundred keV: this result is obtained with nonrelativistic kinematics by assuming a typical mass of $100\,\mathrm{GeV/c^2}$ and a velocity of $10^{-3}\,\mathrm{c}$ for a WIMP. Light dark matter models (mass below $1\,\mathrm{GeV/c^2}$) can also be probed directly, favoring electron scattering over nuclear scattering as momentum transfer is more favorable to electrons at this mass scale. Additionally, scattering on light nuclei is a viable option, with superfluid helium detectors being explored as a potential application [8, 9, 10]. In both scenarios, as the momentum transfer is well below the electroweak scale, the interaction mechanism can be regarded as a contact interaction. This enables the exploration of numerous high-energy-specific models, as they exhibit nearly identical phenomenology at such low-energy scale. Throughout the rest of this article, if not explicitly specified, it is implied that the signal of interest of a WIMP interacting with matter is a nuclear recoil.

The event rate in a direct detection experiment is strongly dependent on the velocity profile of dark matter and the local dark matter density. The differential scattering rate as a function of recoil energy E_R in a target detector can be written as

$$\frac{dR}{dE_R}\left(E_R, t\right) = N_T \frac{\rho_0}{m_\chi} \cdot \int_{v > v_{\min}} v\, f(\vec{v}, t) \frac{d\sigma}{dE_R}\left(E_R, v\right)\, d^3v, \tag{1}$$

where N_T is the number of target nuclei, m_χ is the WIMP mass, ρ_0 is the local dark matter density, $v = |\vec{v}|$ and $f(\vec{v}, t)$ are, respectively, the WIMP velocity and velocity distribution in the experiment's rest frame, σ is the scattering cross section on the nucleus, and $v_{\min}$ is the minimum WIMP speed that can produce a recoil of energy E_R.

The approximate number of interactions inside a detector's active medium can be roughly estimated by simplifying equation (1) assuming a velocity distribution f peaked at an average value $\langle v \rangle$ and integrating in energy and time:

$$N_{\text{events}} \approx N_T \frac{\rho_0}{m_\chi} \langle v \rangle \left\langle \sigma_{\chi - N} \right\rangle \Delta t. \tag{2}$$

For an experiment with target mass number A, active mass M, and total live time Δt, the expected number of events is

$$N_{\text{events}} = 0.135 \cdot \frac{1}{A} \cdot \left(\frac{M}{1\,\mathrm{t}}\right) \cdot \left(\frac{\rho_0}{0.3\,\mathrm{GeV/cm^3}}\right) \cdot \left(\frac{100\,\mathrm{GeV}}{m_\chi}\right) \cdot \left(\frac{\langle v \rangle}{2.38 \times 10^7\,\mathrm{cm/s}}\right) \cdot \left(\frac{\left\langle \sigma_{\chi - N} \right\rangle}{10^{-43}\,\mathrm{cm^2}}\right) \cdot \left(\frac{\Delta t}{1\,\mathrm{yr}}\right), \tag{3}$$

where $\langle \sigma_{\chi - N} \rangle \sim \mu^2 A^2 \langle \sigma_{\chi - n} \rangle$ is the energy-averaged WIMP-nucleus cross section expressed in terms of the WIMP-nucleon cross section $\langle \sigma_{\chi - n} \rangle$ and of the ratio of reduced masses for the WIMP-nucleus and WIMP-nucleon systems μ.

For argon detectors ($A = 40$), assuming a WIMP of mass $100\,\mathrm{GeV}$, a dark matter density of $0.3\,\mathrm{GeV/cm^3}$ and an average velocity in the range of intragalactic velocities [11], the equation yields

$$\frac{N_{\text{events}}}{M \cdot \Delta t} \simeq 4 \frac{\text{events}}{\mathrm{t \cdot yr}} \cdot \left(\frac{\sigma_{\chi - n}}{10^{-46}\,\mathrm{cm^2}}\right). \tag{4}$$

With $10^{-46}\,\mathrm{cm^2}$ being the value for the WIMP-nucleon cross section presently probed by direct detection experiments. This quick estimation explains why many frontier experiments expect a handful of events over their total exposure. The ultrararity of WIMP events combined with their extremely low-energy release sets the challenge for direct dark matter detection, requiring high sensitivity, high exposure, and ultra-low background to be reached with refined passive and active background rejection techniques.

Given the small cross section, multiple interactions within the detector by a dark matter particle are ruled out. Hence, the fundamental signature of a dark matter signal consists of a nuclear recoil spectrum of single-scattering events. Equation (1) can be approximated by [12]

$$\frac{dR}{dE_R} \approx \frac{R_0}{E_0 r} \cdot \exp\left(-\frac{E_R}{E_0 r}\right), \tag{5}$$

where E_0 is the most probable incident kinetic energy of a dark matter particle, r is a kinetic factor dependant on WIMP mass m_χ and nucleon mass m_N, equal to $4m_\chi m_N/(m_\chi + m_N)^2$, and R_0 is the integrated event rate. Provided that sufficient statistics are accumulated in a direct detection experiment, the recoil spectrum can be used to infer the mass of the WIMP.

Another key signature is the expected annual modulation provoked by Earth's rotation around the Sun, which induces a seasonal variation of the total event rate. Although the amplitude of the modulation is expected to be small $\simeq$5%, the period is known to be exactly one year with a 150 d (June 2) phase, when Earth's velocity aligns with solar velocity [13]. The Earth's motion also creates a "wind effect" measurable as a forward-backward asymmetry in the detector in a directional measurement, resulting in a further distinctive signature to correctly identify WIMPs, especially against energetic neutrino-induced nuclear recoils.

1.3. The Fight Against Background

All direct detection experiments searching for WIMP dark matter must be carefully designed to ensure that the background level is at least as low as to match the desired sensitivity, which depends on the total exposure (active mass $\times$ live time) of the experiment. The signal-to-background ratio is extremely important for any rare-event experiment to achieve the significance required for a discovery claim [14]. For any direct detection experiment, the fight against background heavily influences all experimental aspects, from the design of the experimental apparatus to the specific analysis techniques employed to extract results from the collected data. The most obvious necessity is shielding from cosmic rays, which is accomplished by building underground detectors. To further reduce the impact of cosmic rays, active shielding is often employed in the form of a nested detector structure.

Background sources can be divided into internal and external. Internal sources refer to radioactive impurities or contaminants in the active medium, in the detector components and on its inner surfaces. External sources are cosmic rays, neutrinos, and ambient radiation from the surroundings of the experiment.

For argon, most decays do not directly constitute background thanks to particle identification based on pulse shape discrimination (PSD). As described in detail in Section 2.2, provided enough light is available, PSD can easily differentiate between a signal produced by an electronic recoil (ER), i.e., the energetic ionization of an electron from an argon atom, and a nuclear recoil (NR) in which an incoming particle transfers some of its energy to the whole argon nucleus, which moves while followed by the electronic cloud.

The very abundant β and γ decays from long-lived natural or cosmogenically activated radioisotopes (^{238}U, ^{232}Th, ^{39}Ar) and their progeny produce ERs or ER-like signals and can be easily rejected with PSD. α particles, on the other hand, can mimic an NR signal, usually with energies much higher than those in the WIMP region of interest. However, some processes are possible which lead to an indistinguishable background (e.g., an α particle losing most of its energy in the detector's walls before entering liquid argon). To mitigate such background, fiducial position cuts are adopted in argon experiments, excluding a volume close to the detector's inside wall. Position cuts are also capable of removing events constituted by a combination of an ER and Cherenkov light produced in materials surrounding the detector (PTFE, quartz, etc.), which can result in an NR-like signal and can significantly contribute to background otherwise [15]. Fiducial position cuts create the requirement for 3D reconstruction in a low-background dark matter detector.

The most insidious source of background is neutron radiation. Neutrons can produce an NR indistinguishable from the one induced by a WIMP. They are produced by fission reactions of radioisotopes (radiogenic neutrons) or in spallation reactions induced by cosmic muons close to the site of the experiment. To reduce radiogenic neutrons, it is important to select materials for the experiment construction with low uranium and thorium content. At the same time, a passive shield (usually of water) is installed to absorb environmental neutrons. Muon-induced neutrons are strongly suppressed by placing the experimental setup in underground laboratories; active veto systems are commonly used to record interactions by the remaining component of the muon flux that are cut off by an anticoincidence system or during data analysis. Neutrons can be also discriminated by event topology, as the high interaction cross section usually results in multiple scatter events. Very effective neutron background reduction is achieved by making use of a specialized neutron veto system based on materials with a high cross section for neutron capture, like boron or gadolinium, capable of producing a clear signal for anticoincidence when absorbing a neutron [16]. In this way, single-scattering neutrons in the detector, which would otherwise account for background, can be captured by the veto system and be rejected by anticoincidence. The veto system must be designed in such a way as to fully encompass the target, creating a nested configuration that avoids blind corridors for neutrons.

One notable source of background is coherent elastic nuclear scattering from neutrinos, observed for the first time by the COHERENT experiment [17]. Most of the neutrino-induced NR spectrum falls below the typical energy threshold of current detectors, resulting in a negligible contribution to the total background. However, the steady trend in subsequent experiments of increasing the experimental exposure, while reducing the radioactive background, will eventually lead to neutrino-induced NRs becoming the main source of background, posing a threat to further explorations. As the resulting signal is identical to a WIMP-induced event, this background sets a limit to the sensitivity which can be probed with standard techniques [18, 19], and hence, it is referred to as a neutrino floor. To evade it, future experiments will have to adopt new discrimination methodologies. With high enough statistics, a few different approaches are viable: discrimination based on annual modulation of dark matter and neutrino signals combined [20], on daily modulation of dark matter signals [21] or combining data from detectors with different targets [22]. A prospective approach will be reconstructing the energy spectra of neutrinos and dark matter, as they can in theory be distinguished with high enough statistics. To statistically discriminate neutrinos in this manner, the minimum number of events required is between a few thousand and a million, depending on systematic uncertainties of the neutrino flux [22]. For low statistics scenarios, the most promising approach is via directional discrimination [23, 24], as from the Earth the WIMP flux is expected to have a privileged direction due to the motion of the solar system in the galactic medium.

Parameter	Value
Emission peak	128(10) nm
Density (liquid)	1.4 g/cm^3
Boiling point	87.3 K
Scintillation W-value-	19.5 eV
Scintillation photon yield[1]	51 ph/keV
Singlet deexcitation time	6(2) ns
Triplet deexcitation time	1.6(1) μs
Radiation length X_0	14.0 cm
Rayleigh length[2]	95 cm
Absorption length[2]	>200 cm
Refraction index[2]	1.38

TABLE 1: Notable liquid argon properties [25]. [1]At null electric field. [2]For 128 nm light.

2. LIQUID ARGON AS DETECTION MEDIUM

Liquid argon (LAr) is an excellent choice as an active medium for particle detectors (Table 1). Argon in the condensed phase provides high density, high electron mobility, high dielectric rigidity, and the possibility of removing through filters electronegative impurities to a level below 1 ppb (measured as O_2-equivalent contamination). These properties make LAr excellent for detector applications in which electrons are drifted and collected, such as time projection chambers [26], the only drawback being the requirement for a modest cryogenic system in order to maintain it, since argon liquefies at 87.3 K at atmospheric pressure. Moreover, LAr is a bright scintillator, emitting ultraviolet light (to which LAr is highly transparent) with a yield of about 50 photons/keV. Scintillation light is usually converted with a wavelength-shifting material to wavelengths in the optical spectrum, to match the efficiency peak of common photon sensors. The light pulse produced by scintillation can be described by two exponential components with decay times on very different time scales. As the ratio of fast to slow components depends on the linear energy transfer dE/dx (LET) of the incident radiation, PSD techniques can be efficiently applied for particle identification [27, 28]. This property of liquid argon makes it a compelling technology for dark matter research [29].

2.1. Ionization and Scintillation Models

A particle interaction in LAr induces a measurable excitation and ionization of the medium, in the form of a cloud of excitons (Ar^*) and electron-ion couples ($Ar^+ + e^-$) produced in proximity of the interaction locus. These quickly form excimers (Ar_2^*) or ionized dimers (Ar_2^+), respectively, with other argon atoms. A fraction R of the population of Ar_2^+ dimers recombines with a thermalized electron forming additional Ar_2^* excimers. In the absence of an external electric field, most models assume $R = 1$ (all ionized dimers recombine), the effect of escaping electrons being neglected as it is below a few percent [30]. The application of an external electric field allows the collection of ionization electrons, at the cost of reducing the recombination fraction R [31, 32]. Ar_2^* excimers are formed in either singlet or triplet excited states, noted as $^1\Sigma_u^+$ and $^3\Sigma_u^+$, respectively. The two states have approximately the same energy with respect to the ground state, decaying by the emission of a 128 nm photon. However, they do so on two largely different time scales [33] of 6 ns for $^1\Sigma_u^+$ and 1.6 μs for $^3\Sigma_u^+$, as the first-order transition to the ground state for the latter is forbidden.

The detection of scintillation and ionization results in signals proportional either to the number of emitted photons, $S1 \propto N_{\text{ph}} = N_{\text{ex}} + RN_i$, or to the number of free electrons, $S2 \propto N_e = (1 - R)N_i$, where R is the charge recombination fraction for a given particle species, energy, and electric field. Both N_{ph} and N_e are subject to statistical fluctuations, however not independently, as their sum is constrained by the total energy transferred to the medium by the particle. Indeed, the linear combination of $S1$ and $S2$ with suitably chosen coefficients is proven to be a good estimator of the energy released in the interaction, providing a better resolution with respect to each of the two signals separately [34].

For direct detection of dark matter, the characterization of the medium's response to nuclear and electronic recoils is particularly relevant for signal identification and background rejection. With respect to ERs, nuclear recoils suffer from a reduced yield for both scintillation and ionization caused by elastic scattering of the recoiling nucleus on the medium nuclei, which results in thermal energy loss. This quenching effect is also valid for α particles and different atomic species and is well described by the Lindhard model [35]. A more comprehensive model by Mei [36] expands Lindhard's by introducing a high-energy quenching term associated with a saturation effect originally described by Birks [37] and caused mainly by biexcitonic collisions, which provide a nonradiative channel for energy dissipation. The different processes undergone by electrons and nuclei moving through LAr result in a relative variation of the ionization-to-scintillation ratio ($S2/S1$) between ERs and NRs. This allows for the identification of the ionizing particle from the combined measurement of both deposition channels.

As stated above, S1 and S2 exhibit a dependence on the strength of an externally applied electric field, affecting both charge and light yields, ER/NR discrimination power, and energy resolution. An extensive study on the topic was carried out by the SCENE experiment [38], also notably hinting at a possible signal dependence upon the direction of the ionizing particle track for low-energy nuclear recoils. For minimum ionizing tracks, the effect is well understood within the columnar recombination model [39], which assumes ionization around the track shaped as an infinitely long column, dense of ions and electrons. With an electric field, the average time spent by electrons in the columnar cloud of ions, and therefore the recombination fraction R, depends on the

angle of the column, with minimum (maximum) recombination achieved with a direction of the track perpendicular (parallel) to the direction of the electric field. At low energies, the ionization cloud is better described as a localized box following a model by Thomas-Imel [40]. Being isotropic, the box model intrinsically prohibits any directional dependence. The ReD experiment [30] has recently characterized this directional dependence for nuclear recoils with an energy of 70 keV, using an intermediate model between columnar and box ionization by Cataudella et al. [41]. ReD reported strong constraints on a directional effect on this energy scale, which would appear to be hardly usable in a future kton scale argon detector for discrimination against the neutrino floor [42].

2.2. Particle Identification from Scintillation (Pulse Shape Discrimination)

While particle identification is possible from the relative measurement of ionization and scintillation produced in the medium, the distinctive scintillation properties of LAr can be exploited to provide significantly higher discrimination of ERs from NRs, especially compared to the heavier xenon, which is also extensively used for direct dark matter detection. The reason lies in the large separation of the two decay time constants characterizing the singlet and triplet excited states, of two orders of magnitude larger for argon than for xenon. The relative contribution of the short to long component in the scintillation pulse can thus be used to effectively infer the nature of the incoming radiation. Many different approaches are successful, all involving the definition of a parameter that maximizes the separation between ERs and NRs. The most common techniques are as follows: (A) the measurement of the prompt light fraction, (B) likelihood-based discrimination, (C) feature identification in frequency space via FFT, (D) measurement of the rate of change of the signal, or (E) machine or deep learning techniques. These methods are collectively known as pulse shape discrimination (PSD). All PSD techniques strongly rely on efficient light collection from argon scintillation, as they are based on differences in the LAr scintillation profile, which may be statistically fogged by Poissonian fluctuation if not enough light is collected. This is true, especially at lower energies, and has a direct effect on the minimum threshold achievable by experiments. Finally, PSD is also negatively affected by electronic noise, which effectively widens the ER and NR distributions increasing their overlap and reducing discrimination power.

The most commonly used PSD parameter in LAr experiments is the prompt light fraction f_{prompt}, typically defined as the fraction of light collected up to a time τ_{prompt} over the total scintillation light, with τ_{prompt} chosen as to optimize the discrimination power. In Figure 1(a), events from the calibration campaign of the DarkSide-50 experiment are reported as an example of the separation between NRs and ERs obtainable with LAr. DarkSide-50 is an underground LAr-based experiment, which will be presented in detail in Section 5.1. In the figure, events obtained with a neutron source are plotted with respect to the f_{prompt} variable and measured scintillation light ($S1$). Neutron-induced nuclear recoils populate the upper band with a high value of f_{prompt}, while electron recoils are characterized by lower values of f_{prompt}. In the figure, f_{prompt} is noted as f_{90}, as a prompt time of 90 ns is chosen. With this method, the DarkSide-50 experiment observed 1.5×10^7 ER events with no leakage for nuclear recoil acceptance (NRA) of 90% [44]. A similar method was used in [28] to separate electron and nuclear recoil events, with a leakage of less than 2.7×10^{-8} (90% CL) for 90% NRA. The performance of the prompt fraction method, also compared to those obtained with a likelihood analysis, was thoroughly studied with data from the 3.3-ton target mass DEAP-3600 detector (Section 5.2), showing that a leakage probability of 10^{-10} can be reached at 90% NRA with a sufficient light yield [45]. Finally, the information from PSD can be combined with discrimination based on the S2 to S1 ratio to further decrease ER leakage (Figure 1(b)).

2.3. The Quest for Low-Radioactivity Argon

Atmospheric argon (AAr) is intrinsically radioactive due to the presence at an activity of 1 Bq/kg [46] of the radio-isotope ^{39}Ar, a β-emitter with an end point of 565.5 keV and a half-life of 269 yr. Electrons from ^{39}Ar decays produce electron recoils, which can be rejected by PSD and only result in a source of background at very low energies. However, the contamination of ^{39}Ar in the active detection medium would limit the maximum size of the detector due to pileups in the acquisition pipeline, effectively posing a limit to the upscaling of a system and bounding the maximum exposure obtainable from a direct detection experiment.

AAr is primarily composed of the stable isotope ^{40}Ar, with traces of ^{39}Ar generated in the upper atmosphere by cosmic ray interactions through ^{40}Ar(n,2n)^{39}Ar reactions. Centrifugation, differential thermal diffusion, and isotope separation, are employed to decrease the concentration of ^{39}Ar in argon. While effective, these methods can be expensive and time-consuming due to the precision required for isotope separation and the complexity of the processes involved. On the other hand, the bulk of atmospheric ^{40}Ar comes from the decay of ^{40}K within the Earth, with a significant portion remaining underground. Thus, one could presume argon from underground wells to be less contaminated by ^{39}Ar due to the effective attenuation of cosmic rays by rocks. However, studies have shown that ^{39}Ar can also be produced underground through reactions involving radiogenic neutrons and stable potassium. The concentration of ^{39}Ar in crustal argon is expected to be comparable to atmospheric levels, but variations exist due to differing uranium and thorium content in rocks, resulting in underground ^{39}Ar levels ranging from substantially lower to notably higher than atmospheric values [47]. The Earth's mantle, with much lower uranium and thorium levels compared to the crust [48], is anticipated to contain significantly less ^{39}Ar in its argon content, potentially several orders of magnitude lower than crustal argon. While direct extraction from the mantle does not seem feasible with current technology, harnessing mantle-derived gases from accessible locations, such as in deep gas wells, allows for the procurement of extremely radiopure argon.

The design and operation of large LAr dark matter detectors such as those of the DarkSide family (see Section 5) is possible because of the discovery of low-radioactivity argon in underground CO_2 wells [49], most likely of mantle origin [50]. Low-radioactivity underground argon (UAr) has already been employed in DarkSide-50, which demonstrated that the activity of the UAr sample was at least 1400 times lower than that of AAr [51]. DarkSide-20k is the first ton-scale experiment to use UAr as a target [52]. Future low-energy experiments using argon will require an increasing mass of UAr to contain the ^{39}Ar event rate, of

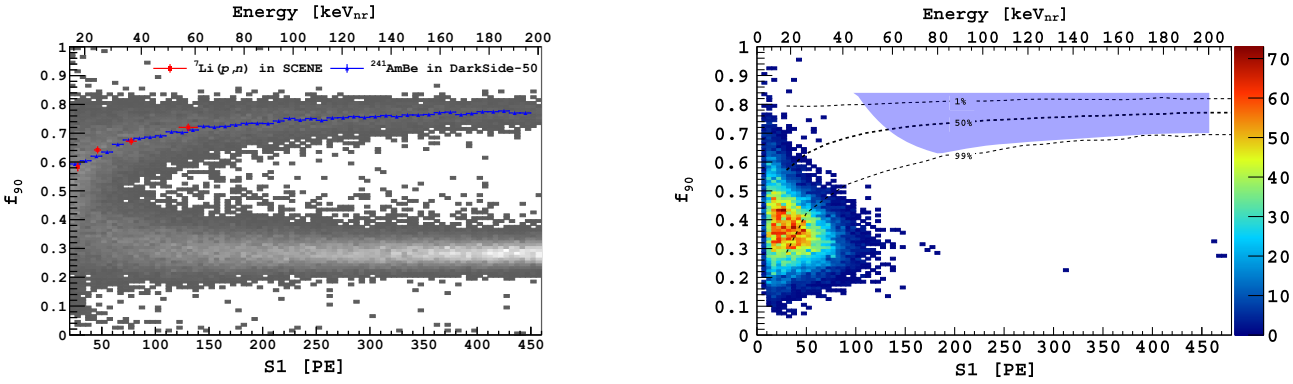

(a) (b)

FIGURE 1: (a) In grey, events from the DarkSide-50 (DS-50) experiment calibration with a ^{241}Am^{9}Be neutron source, provoking nuclear recoils in the TPC. On the vertical axis is the PSD parameter f_{90} (f_{prompt} with $\tau_{\text{prompt}} = 90$ ns), optimized for the DS-50 detector; on the horizontal axes is the measured scintillation (lower axis) and the corresponding energy in nuclear recoil equivalent (upper axis). The two populations at f_{90} of about 0.7 and 0.3 are nuclear recoils (NRs) and electron recoils (ERs), respectively. Separation of the two populations above $\sim$30 keV$_{\text{nr}}$ is excellent. The data points represent the f_{90} median for NRs measured by DS-50 and the small LArTPC of the SCENE experiment [38]. Figure reprinted from [43]. (b) Distribution of events in the f90 vs S1 plane from the 532-day dark matter search of DS-50 surviving all analysis cuts, including a selection based on the S2 to S1 ratio and radial position cuts. The blue area indicates the WIMP search region; zero events are found. The dashed lines correspond to 1%, 50%, and 99% f90 acceptance contours for nuclear recoils, obtained from the ^{241}Am^{9}Be calibration. Figure reprinted from [15].

the order of several hundred or even 10^3 tons (such as Argo [53] and possibly in one of DUNE's future modules [54]); furthermore, disparate fields of physics would benefit from broader availability of low-radioactivity argon [55, 56], such as precision measurement of the coherent elastic neutrino-nucleus scattering in COHERENT [57], low-energy neutrino telescopes, environmental measurements based on argon-argon radiometric dating, and neutrinoless double beta decay in LEGEND [58, 59]. This makes the procurement of large masses of low-radioactivity underground argon and/or the development of isotopic separation techniques a significant challenge for future low-threshold LAr detectors.

3. ARGON TECHNOLOGIES FOR DARK MATTER SEARCHES

Liquid argon exhibits several advantageous properties that collectively make it an attractive candidate for direct dark matter searches, offering multiple avenues for detecting and studying potential interactions between dark matter particles and ordinary matter. It offers dual detection channels by generating scintillation light and ionization upon interaction with WIMPs, enabling a more comprehensive approach to signal identification and background rejection. Additionally, its low radioactivity, scalability potential, high density, and effective signal readout contribute to its suitability for constructing sensitive detectors capable of reaching the hundred- and even kilo- ton scale.

The technologies presented in this section reflect different design choices based on the readout of a single channel or both: single-phase scintillation detectors and two-phase time projection chambers are the most established detectors in active and terminated experiments, and both are presented in this section. Technical details on the light collection, as well as future developments for these established technologies, are deferred to later sections. It is worth noting here that every experiment in which light is measured has to deal with the problem of wavelength mismatch between argon emission and the acceptance window for commercially available photon counters, which is usually addressed in the LAr experiment by implementing a wavelength-shifting substance in the detector with deposition on surfaces and thin sheets or directly into the active medium by argon doping.

3.1. Scintillation Detectors

The simplest design for a particle detector based on liquid argon is a single-phase scintillation detector, which consists of an LAr scintillator mass coupled to an array of photon detectors (see Figure 2(a)). By discarding the ionization channel, no external electric field is required, the maximizing recombination of electrons with argon ions and hence achieving maximum light yield with respect to other detector classes. Furthermore, the absence of a charge collection system and electrodes for field generation results in useful space for active light detection, which can reach a very high coverage of close to 100% (4π readout).

A detector's light yield is a key performance parameter, influencing the energy threshold, resolution, and PSD discrimination power. The typical photon collection efficiency achieved by current detectors is about 20% with light yields in the range of 7–10 photoelectrons/keV (for electron recoils). Light yield is strongly dependent on the photon-collection efficiency and the quantum efficiency of the photon detectors used. The former may be improved by efficient light guiding, optical coupling, and a high total photosensor coverage; the latter by developments in the field of photon-counting devices. The reconstruction of event

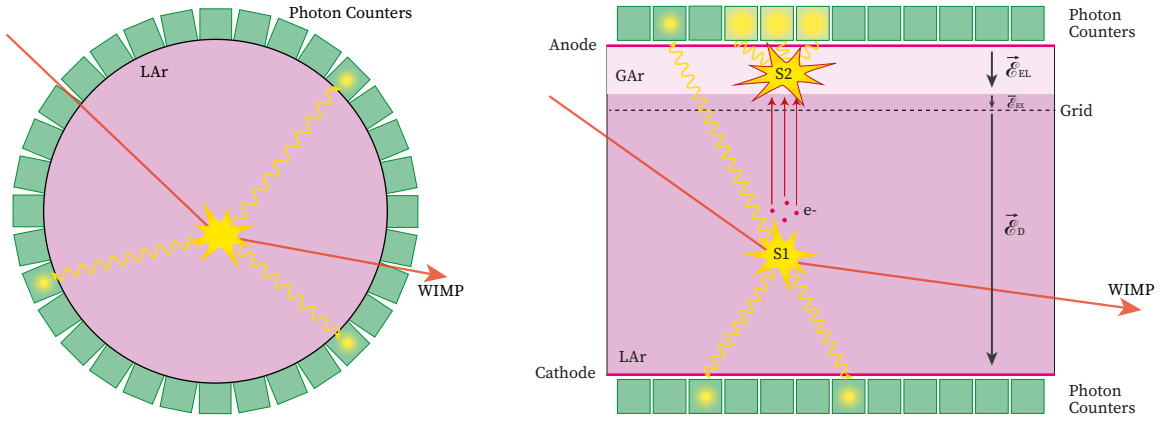

(a) (b)

FIGURE 2: (a) Scheme of a liquid argon scintillation detector. The interaction of a WIMP produces a nuclear recoil, detected by measuring the scintillation light with adequate photon detectors. (b) Working principle of an argon dual-phase TPC. A recoil event in the active volume produces scintillation photons and ionization electrons. The former are detected by the photosensors resulting in the $S1$ signal. Ionization electrons are drifted toward the gaseous region by the drift field $\vec{\mathcal{E}}_D$ and then extracted from the liquid by the extraction field $\vec{\mathcal{E}}_{\rm EX}$. In gas, the electroluminescence field $\vec{\mathcal{E}}_{\rm EL}$ results in the production of photons proportionally to the extracted charge. The associated signal detected by the photosensors is called $S2$.

locations is possible, with a few cm resolution, by analyzing the timing and spatial distribution of detected photons. Position reconstruction is crucial for fiducialization and the rejection of surface background. Finally, it is worth mentioning that scintillation detectors cannot rely on the information of ionization-to-scintillation ratio ($S2/S1$) for ER/NR discrimination and they must rely only on PSD. An example of a scintillation detector with LAr comes from DEAP-3600, discussed in Section 5.2.

3.2. *Time Projection Chambers*

LAr Time Projection Chambers (LArTPC) are a class of detectors designed to measure the ionization channel in LAr via drifting and collecting electrons; simultaneous measurement of scintillation through photon detectors can provide either triggering or triggering plus energy information.

To collect charge, ionization electrons must be moved by an electrostatic field from the interaction locus within the active volume to a suitable readout system. In an LArTPC, this is achieved by parallel electrodes which confine the active region. Long drifts are allowed by the fact that argon does not attach electrons so that electron lifetime can be improved by continuously filtering electronegative impurities (such as molecular oxygen and nitrogen). With an electric field of (100–500) V/cm in LAr, electrons drift at a speed (9–11) m/ms, and a lifetime of 3.0 ms can be achieved by reducing electronegative impurities to 1 ppb (O_2-equivalent concentration) at 500 V/cm [25]. Disuniformities in the drift field negatively impact electron collection and introduce jitter and loss of temporal resolution. Therefore, a field cage is typically used alongside the field-generating system of an LArTPC to correct for border effects and ensure parallel field lines across the whole active volume. A common design choice for the field cage involves a set of conductive rings surrounding the detector's inner volume, with each ring set at a different voltage via a voltage divider. For high-energy, non-dark-matter, applications ($\gtrsim$10 MeV), oriented wire planes, pads, pixels, or other charge collection instrumentation can be used to form a charge-sensitive surface from which a 2D image of a track inside the detector can be reconstructed. Independently, light from argon scintillation can be readout with photon detectors, providing the start time of the event t_0 and a fast trigger, as the fast fraction of the light reaches the photon detectors in a few nanoseconds, depending on the detector's size. The temporal difference between the scintillation and the ionization signals (drift time) can be used to retrieve the coordinate of the event in the direction parallel to the drift field, for a full 3D reconstruction of tracks and vertices.

Besides their remarkable imaging capabilities, constrained by readout granularity and electron diffusion, LArTPCs are also excellent calorimeters. They precisely measure local energy depositions, which is critical for electron/γ separation and particle identification. Charge integration enables the reconstruction of energies from complex events, while dE/dx measurement along the track allows for momentum measurement. If enough light is collected, luminous information can be used to improve the energy measurement and provide additional discrimination through PSD, but the design of LArTPCs inherently imposes restrictions on the optical coverage caused by the encumbrance of the field-generating and charge collection systems, and the difficulty of placing photon detectors close to high-voltage surfaces. The design of LArTPCs presently adopted by modern experiments can be further improved by enhancing the light collection, reducing optical interference from electrical and charge collection components, and increasing the coverage and quality of photon detectors.

Finally, as the typical charge yield in liquid argon is in the order of 40k e^-/MeV, low-energy applications such as direct detection of WIMP require some form of charge amplification and cannot rely on direct charge collection. The most widely used technology, in which charge is converted to light with an advantageous conversion factor, is the two-phase TPC.

3.3. Two-Phase Time Projection Chambers

A two-phase argon time projection chamber is an LArTPC that implements a charge-readout technique based on the electroluminescence phenomenon in gaseous argon. A schematic of this kind of detector is presented in Figure 2(b). The scintillation light of argon is read out in the same way as described in the previous paragraphs, and the free electrons produced during an event are drifted upward by an electric field, analogous to a single-phase LArTPC. At the end of their journey, electrons are extracted into a thin layer of gas confined within a diving-bell structure. The gas is constantly replenished to maintain the equilibrium between gas and liquid, usually by a resistive boiler. The extraction is possible by an electric field on the order of 5 kV/cm, much stronger with respect to the field required to drift electrons toward the gas. This is necessary to overcome the extraction potential of the liquid-gas interface, which acts as a capacitive surface. In gas argon, an electric field of the same order of magnitude as the extraction field is operated to have electrons produce scintillation light by electroluminescence, without generating further ionization. This results in a light signal proportional to the charge extracted from liquid argon ($S2$). In this way, both scintillation and ionization can be read out by photon detectors.

To produce two uncoupled field values with different orders of magnitude in the active region (drift field) and extraction/amplification region, an additional electrode must separate the two regions. A wire grid (or mesh) is used as it must allow the passage of electrons, and its opacity directly influences both charge extraction and field uniformity.

Light guiding and collection are crucial in a two-phase LArTPC. Specifically, the luminous signal associated with ionization is always produced at the very top of the detector, and the most efficient location for photon detectors is close to the gas layer. This requires a transparent electrode for field generation, which can be achieved by thin depositions of suited conductive materials, an example being indium tin oxide (ITO). High-performance reflectors can complete the optical system in parts of the detector where photon-counting devices are too impractical (e.g., on lateral walls of the TPC, close to the field cage) to improve the total light yield, with current detectors achieving a light collection efficiency similar to that achieved by single-phase detectors.

3D reconstruction is analogous to single-phase TPCs. The vertical coordinate, which by design must be parallel to the direction of the drift, is inferred from the drift time, i.e., the time difference between $S1$ and $S2$ signals. For low-energy point-like tracks (as those expected from a WIMP-induced nuclear recoil), the horizontal projection of an interaction vertex is obtained as the barycenter of the light distribution of the $S2$ signal on the upper array of photosensors. An additional significant aspect of LArTPC is that the simultaneous measurement of both light and ionization channels allows for the discrimination of incident particles by combining information from PSD and S2/S1 ratio, further enhancing the already outstanding capabilities of PSD (Figure 1(b)). The excellent charge extraction and efficient collection of scintillation photons, combined with LAr scintillation properties and good spatial resolution for precise fiducialization, make the two-phase LArTPC well equipped for ultra-low background applications.

The dual-phase TPC can achieve detection thresholds in the sub-keV range by relying solely on the ionization signal ("S2-only" mode) [60, 61, 62, 63, 64, 65, 66]. At very low energies, the scintillation signal can no longer be observed, but the high survival probability characterizing drift in high-purity argon, coupled with the nearly 100% efficient extraction and the high amplification obtained in gas, enables the detection of single electron signals and provides centimeter-level resolution for reconstructing the interaction position on the plane perpendicular to the electric field. Additionally, the system efficiently rejects multisite signals associated with multiple scattering particles, which are inconsistent with those induced by dark matter. The inner detector of DarkSide-50, discussed in Section 5.1, is an example of a two-phase LArTPC for direct detection of dark matter.

Finally, it is worth noting that the two-phase time projection chamber paradigm finds extensive application not only with liquid argon but also in xenon dark matter experiments, with two-phase LXeTPCs holding the best exclusion limits for WIMPs across a wide mass range at the time of publication (Section 5). Most of the principles and techniques described in this section are directly translated to LXeTPCs due to the similarities between argon and xenon. However, their differences in aspects such as scintillation wavelength, atomic mass, nuclear spin, and boiling points have implications on both design optimization and physics reach.

3.4. Novel Detector Technologies

A completely different approach with respect to those presented above is being developed by the scintillating bubble chamber (SBC) Collaboration [67]. The working principle of a bubble chamber is to maintain a fluid in a superheated state, so that incident radiation generates nucleation points in the form of local ionization, resulting in the formation of a bubble (or a track of bubbles), detectable by measurement of acoustic oscillations and cameras. Bubble chambers are successful detectors in low-mass spin-dependent dark matter searches because they are essentially blind to electron recoils. This is possible because the stopping power for electrons is lower than for nuclei, and the threshold for bubble formation can be adjusted to be insensitive to ERs with an appropriate choice of thermodynamic parameters [68].

The scintillating bubble chamber prototype by SBC exploits superheated LAr instrumented with acoustic detectors, cameras for bubbles, and SiPM optical readout for argon scintillation light [69]. Measuring both bubbles and scintillation combines the strengths of both technologies: ER-blindness of bubble chambers and high-resolution energy measurement from argon scintillation light. The collaboration has already validated the idea on a small-scale xenon prototype [70] and the first 10 kg LAr detector is in the commissioning phase.

4. LIGHT DETECTION TECHNIQUES: STATUS AND PROSPECTS

Light detection is a key link in the readout pipeline for any scintillator-based detector. For argon, the two main complications for any light detection system arise from the very short wavelength of the scintillation light of argon and the complication of working with highly sensitive instrumentation at cryogenic temperatures. In fact, most commercial solutions available for photon detection are not sensitive or still exhibit a very low detection efficiency in the vacuum ultraviolet (VUV) range in which argon scintillation falls. On the other hand, the cryogenic environment poses a challenge as electronic and mechanical components of photon detectors show a temperature-dependent response and performance, and often specific technologies require (or have required) careful development to be adapted to the cold environment.

4.1. Photomultiplier Tubes (PMTs)

PMTs are versatile light detectors that have played a pivotal role in scientific and industrial applications for several decades. PMTs remain fundamental to fields such as particle physics, astronomy, medical imaging, and fluorescence spectroscopy due to their single photon sensitivity, fast response time, and wide dynamic range. The principles of operation of the photomultiplier tube are the photoelectric effect and electron multiplication. When a photon strikes the photosensitive cathode of a PMT, it ejects an electron via the photoelectric effect. This primary electron is then accelerated and focused toward a series of dynodes, each maintained at a progressively higher positive voltage in a sealed vacuum environment. As the electron impinges on these dynodes, it extracts secondary electrons due to its high kinetic energy, amplifying the total charge flowing through the PMT. This cascade of secondary electrons results in a measurable current at the anode, which is proportional to the incident photon flux. Gains of the order of (or greater than) 10^6 are typical for PMTs, allowing for signal readout without the use of front-end amplifiers.

The main challenge for the use of photomultiplier tubes at cryogenic temperature is the increase of resistivity of both cathode and dynodes, causing loss of efficiency and gain instabilities. Current state-of-the-art phototubes designed specifically for noble liquid applications employ special low-resistivity bialkali photocathodes [71], featuring good low-temperature performance and $\sim$30% quantum efficiency in the visible range and down to 170 nm. This requires the use of a WLS in order to shift the VUV light emitted by argon in the scintillation process. Customized PMTs for noble liquid dark matter experiments also offer a reduced intrinsic radioactive background thanks to the accurate selection of the construction materials, in particular, the PMT body made of Kovar, the stems in the back of the PMT, and the ceramic around the dynodes chain, which are the main source of residual radioactivity [72, 73].

Despite the progress made in the development of cryogenic PMTs for liquid argon, numerous unresolved challenges persist. These hurdles not only hinder scalability but also demand innovative solutions to ensure effective deployment. The foremost challenge lies in achieving cost efficiency without compromising the photon-sensitive area. The ability to scale up while maintaining a reasonable cost per unit of photon-sensitive area remains a significant bottleneck. Another critical concern is the management and reduction of radioactive background levels. The quest for scalability demands not only cost-efficient scaling but also stringent control over the manufacturing process. Starting from the selection of radiopure materials and extending to the meticulous oversight of the manufacturing process, every step is critical. Finally, operational instabilities at cryogenic temperatures stand as a concealed challenge. Observations of operational instabilities at cryogenic temperatures have necessitated proactive measures for stabilization. In fact, a dramatic increase in dark count rate has been reported for cryogenic PMTs operated in liquid argon above a gain of 10^6, which could only be cured by turning off the PMT for several hours [74]. In order to recover the gain required for single photoelectron identification, the devices were equipped with preamplifiers mounted directly on the HV dividers allowing for operation at a lower gain of 10^5. This adaptive approach highlights the need for real-time monitoring and dynamic adjustments to ensure stable and reliable detector performance in extreme environmental conditions.

Addressing these challenges demands interdisciplinary approaches, innovative engineering solutions, and meticulous calibration techniques. Overcoming these hurdles is pivotal in advancing the reliability and efficiency of photon detectors for liquid argon dark matter experiments.

4.2. Silicon Photomultipliers (SiPMs)

SiPMs, a relatively recent semiconductor-based technology for light readout, have gained increasing popularity in the last few decades and are establishing themselves as a direct alternative to PMTs due to their numerous advantages [75]. Differently from PMTs, SiPMs are low-voltage powered, not disturbed by magnetic fields, more compact, and cheaper and usually exhibit a larger photon detection efficiency together with unrivaled photon-counting capabilities. In addition, silicon devices are inherently more radiopure than PMTs [76], and their performances generally improve at lower temperatures. Last but not least, they allow for scalable mass production. For these reasons, many large-scale noble liquid experiments are implementing SiPMs as main photosensors in their detectors [52, 77, 78, 79].

4.2.1. Working Principle and Main Parameters of SiPMs

A Silicon Photomultiplier integrates a dense array of independent Single Photon Avalanche Diodes (SPADs) with quenching resistors, connected in parallel to form a pixelated grid of photosensors, with pixel densities ranging $(10^2$–$10^4)/\mathrm{mm}^2$. When operated above breakdown, each SPAD constitutes a microcell unit, generating a self-sustained charge avalanche upon absorbing incident photons. The self-sustaining nature of the avalanche makes it independent from the number of photons which originated it. In low photon flux applications, SiPMs restore linearity between the flux intensity and signal output: N photons hitting the device simultaneously generate on average $\epsilon \cdot N$ avalanches (ϵ being a global efficiency factor) producing an average output charge pro-

portional to N. Since the SPADs act as individual photon counters, an excellent resolution for single photons can be achieved, with linearity only limited by the number of microcells.

SiPM performances are strongly dependent on the applied reverse bias voltage and temperature. It is common practice to refer to SiPM-related quantities as a function of the overvoltage (OV), which is the bias voltage above the breakdown voltage. The gain depends linearly on the OV and is in the range of 10^5–10^7. For operation at cryogenic temperature, one should note the reduction of the breakdown voltage, due to an increase in the mean free path of charge carriers drifting in the high-field region of a SPAD, resulting in a stronger impact ionization. Nominal gain can be recovered by adjusting the OV. Gain stability with temperature is not an issue for LAr applications as very strict temperature stabilization is anyway required in these detectors.

The shape of the signal is determined by the time it takes for a single SPAD to return to a relaxed state after an avalanche, called pixel recovery time. After a pixel discharge is quenched, a microcell can be thought of as an RC circuit with a characteristic time τ_r, given as a product between the microcell resistance R_q and capacitance C. Typical values for R_q and C are (100–1000) kΩ and (20–150) fF, respectively, so that the pixel recovery time τ_r ranges (10–10^4) ns. A key aspect of the cryogenic use of SiPMs is the technology used for the quenching resistors. Depending on the material chosen, the value of R_q may significantly increase with decreasing temperature, demanding an adjustment of its value to match the requirements in LAr. On the other hand, reducing the value of R_q could prevent the possibility of operating the SiPM at both room and cryogenic temperatures, with obvious disadvantages. The most common choices are metal or polysilicon quenching resistors, with the latter being much more temperature-dependent. The most important parameters for the purpose of using SiPMs to detect LAr scintillation are photon sensitivity, dark counts, and excess noise.

Photon Detection Efficiency

Photon detection efficiency (PDE) is the probability that a photon of a given wavelength λ incident on a SiPM will produce an avalanche, and it determines the sensitivity of a SiPM. PDE can be expressed as follows [75]:

$$\mathrm{PDE}(\lambda, \mathrm{OV}, T) = \mathrm{QE}(\lambda) \cdot P_{\mathrm{trigger}}(\lambda, \mathrm{OV}, T) \cdot G_{\mathrm{ff}}, \tag{6}$$

where $\mathrm{QE}(\lambda)$ is the wavelength-dependent quantum efficiency of a pixel, P_{trigger} is the wavelength-, voltage-, and temperature-dependent probability that an electron-hole pair produced in the depletion region will trigger a Geiger discharge, and G_{ff} is a geometrical factor (fill factor) measured as the fraction of the SiPM active surface over its total surface. The maximum of PDE at ambient temperature with respect to wavelength is found within the optical spectrum for a value exceeding (50–60)% depending on the device [80]. Standard devices have a negligible PDE in the wavelength region of argon emission since VUV photons do not reach the sensitive region. While R&D is still ongoing to improve this aspect, recent specialized technologies already show wavelength sensitivity extending into the VUV spectral region, with PDE of the order of 20% [81, 82]. PDE has a nonlinear nonmonotonic trend with respect to temperature [83], due to physical mechanisms not completely understood as of today. Instead, PDE shows a monotonic increase with OV.

Dark Count Rate

In the absence of luminous stimulation, Geiger discharges can be provoked by thermally generated electron-hole pairs in the depletion region of a SPAD. The rate of such pulses is referred to as dark count rate (DCR) and can negatively impact the trigger efficiency and pulse shape discrimination in direct dark matter detection experiments. When going cryogenic, SiPMs exhibit a great reduction in DCR up to six orders of magnitude from room temperature to 100 K [80] (Figure 3(a)), due to DCR being a thermal process. As DCR can be a source a nuisance in low-energy applications, this behavior makes SiPMs a compelling choice for the light readout of LAr detectors.

Correlated Noise

The excess noise factor depends on the probability that a correlated noise event is generated by a primary avalanche. During a Geiger avalanche in a SPAD, impurities and crystal defects may trap a fraction of charge carriers, which can then be released back into the depletion region after the microcell has returned to its relaxed state. When this happens, the freed charges can produce a correlated secondary discharge, resulting in a delayed signal called an *afterpulse* (AP). Charge carriers trapped and then released very early after a discharge (before the typical recovery time) do not induce a correlated pulse, as the overvoltage across the junction is not yet restored. As a consequence, decreasing the recovery time of a SiPM inherently results in increasing the number of trapped carriers released after or midway recovery, which translates to higher AP probability, and vice versa. At cryogenic temperatures, the AP probability can increase significantly as carrier reemission is a thermally activated process, and a longer reemission lifetime results in a lager fraction of carriers being freed close or after a complete recharging of the cell [80] (Figure 3(b)). Photon generation as a secondary process during the avalanche triggers *optical cross-talk* (CT). These photons have the potential to induce internal CT, by interacting with a neighboring microcell, or external CT, if they escape the silicon bulk and are reflected back triggering a signal in a different SiPM. Both these phenomena have the effect of increasing the number of counts per primary photon. Optical CT can be reduced by introducing opaque trenches between adjacent cells.

4.2.2. Development of Cryogenic VUV-Sensitive SiPMs

Implementing a SiPM readout in liquid argon detectors requires, first of all, a device compliant with cryogenic temperatures. This is more easily achieved for SiPMs with a metal quenching resistor, which usually achieve satisfactory performance at 87 K without

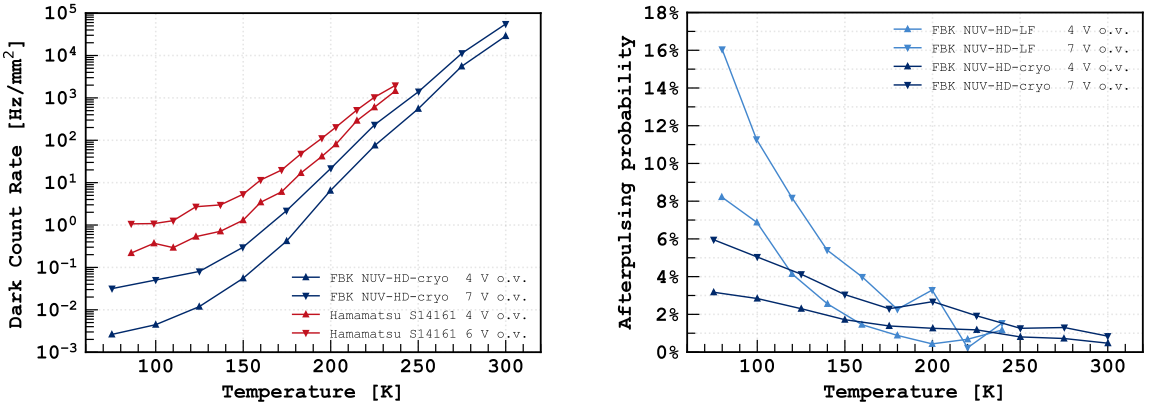

(a) (b)

FIGURE 3: (a) Dark count rate as a function of temperature measured for two devices, an FBK NUV-HD-Cryo SiPM [84] and a Hamamatsu Multipixel Photon Counter [85] operated at different over voltages. (b) Afterpulsing probability as a function of temperature for FBK NUV-HD-Cryo and FBK NUV-HD-LF SiPMs devices at two OV values [84].

further adjustments. An illustrative case is the cryogenic response exhibited by a SiPM array from Hamamatsu's S14161 series, as detailed in [85]. For SiPMs with poly-Si quenching resistors, performance worsens when going cryogenic to the point of rendering the device unusable without any targeted modification. This is due to the strong temperature dependence of poly-Si resistors with respect to metal. Fondazione Bruno Kessler (FBK) had to tackle this challenge in their NUV-HD-Cryo technology by incorporating a tailored quenching resistor into an existing technology, namely, the NUV-HD-LF [80]. The NUV-HD-Cryo series features a distinct production technique that improves (reduces) the AP probability in the cold environment, which can be appreciated in Figure 3(b).

SiPMs designed for cryogenic applications are already accessible in the commercial market, demonstrating performance that matches or surpasses that of PMTs. The next feasible significant advancement toward achieving optimal silicon-based readout in argon detectors involves eliminating the need for a wavelength-shifting material. This requirement poses a major design complication, and it can be circumvented by using SiPMs with sufficiently high PDE in the VUV range. In light of the interest generated within the argon and xenon communities for such devices, several companies have begun an extensive R&D process, with the most active being FBK with their VUV-HD-Cryo series [84, 86] and Hamamatsu with their VUV series at its fourth iteration (VUV4) [81]. To this day, the best commercially available technologies are still limited to about 20% PDE for 128 nm light, making light collection in the optical spectrum with WLSs still preferable in most applications.

Ongoing developments aim at increasing the quantum efficiency of VUV-sensitive devices, with the main limiting factors for efficient collection of VUV radiation currently being the high reflectivity of present devices and very shallow absorption depth in Si (of the order of nanometers). High reflectivity can be cured with VUV-specific antireflective coatings (ARCs) optimized for non-normal incidence and active-surface passivation, i.e., the treatment or coating of the silicon surface to reduce surface defects, which worsen the device's performance. On the other hand, the small absorption depth can be dealt with by carefully designing a device geometry that minimizes the distance between the SiPM surface and the photosensitive volume. A very promising development that could lay the groundwork for future breakthroughs is the backside illuminated (BSI) SiPM. Most of the SiPM technologies discussed in this section are front-side illuminated (FSI); i.e., SiPM electric components and structural elements are on the same side as the sensitive area. The BSI SiPM is an alternative geometry with the sensitive area on the backside of the SiPM: a smooth Si surface without competing elements and maximum fill factor. A completely smooth surface allows for an easy implementation of advanced multilayered ARCs or even 3D-textured ARCs [87]. The concept of backside illumination has already been validated in charge-coupled integrated devices [88, 89], achieving up to 40% efficiency for a wavelength of 178 nm.

4.2.3. Upscaling Challenges

Designing a large-surface SiPM readout is a challenge for future high-mass detectors: due to their small active surface ($\mathcal{O}(1\,\mathrm{cm}^2)$), any ton-scale detector would require an unrealistic number of readout channels without a form of output aggregation. However, readingout multiple SiPMs in a parallel configuration would result in a very high input capacitance to the amplification and readout pipeline, inevitably leading to reduced bandwidth and a lower signal-to-noise ratio. In order to cope with this problem, multiple SiPM cells must be combined into a single analog output using dedicated front-end electronics, which must be compliant with temperatures in the operational range of liquid argon and satisfy stringent radiopurity constraints to be well within the radio-budget of an ultralow background detector.

A modular and easily scalable SiPM-based technology was developed for the optical readout of the DarkSide-20k experiment (Section 5.3), combining 24 1 cm^2 SiPMs on a tile and 16 such tiles into a single unit of (20×20) cm^2 with four readout channels [90]. The 24 SiPMs on a tile are arranged electrically arranged in six parallel branches of four SiPMs in series, to contain the effective capacitance. SiPMs are biassed through a voltage divider, and the output of the SiPM aggregate is processed by a cryogenic low-noise transimpedence amplifier (TIA) [91] that outputs an analog voltage signal to the motherboard of the Photon Detection Unit

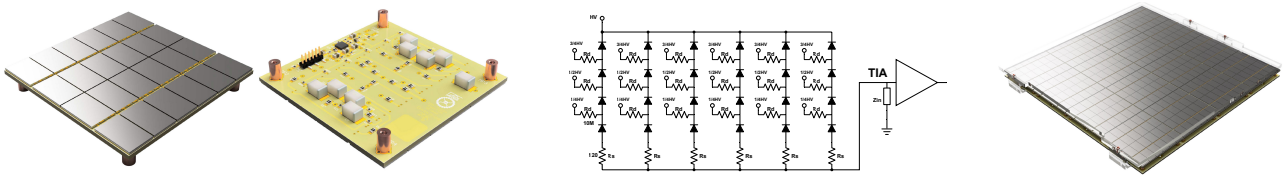

(a) (b) (c)

FIGURE 4: (a) Picture of a DarkSide-20k tile, with a total surface of $(5 \times 5)\,\mathrm{cm}^2$. *Left*: Top view with the 24 SiPMs visible. *Right*: Bottom view of the tile, showing the front-end board. The TIA can be seen on the top left of the picture, along with a data and supply connector. (b) 6p4s connection scheme of a single-SiPM tile, comprised of 24 SiPMs which are readout by a TIA. Each of the four SiPMs in a branch is supplied by a precision voltage divider. (c) Picture of the PDU assembled with all 16 tiles and a total surface of $(20 \times 20)\,\mathrm{cm}^2$. An acrylic transparent cover is temporarily mounted for transport and handling. Pictures reprinted from [92].

(PDU). On the motherboard, the output of the tiles is combined in groups of four by an active-gain adder before finally being fed to a differential transmitter which provides additional amplification. The present design originated from an R&D process from the DarkSide-20k collaboration to build a large-surface SiPM photon detector with an active surface size close to that of a commercially available PMT, and competitive performance. A series of pictures in Figure 4 shows a tile with its electrical scheme and the full assembled PDU.

A compelling prospect for future large-scale light readouts is the digital Silicon Photomultiplier (dSiPM). The fundamental concept of the dSiPM revolves around each SPAD being linked to its dedicated and miniaturized readout electronics, inclusive of a time-to-digital converter (TDC). The first commercial digital SiPM was introduced by Philips [93, 94] in the context of Time-of-Flight PET (TOF-PET). The development of a cryogenic, low-cost dSiPM would circumvent many obstacles related to large-surfaces of analog SiPMs [95]. For instance, integrated signal processing with digital output significantly reduces the burden of managing an increasing number of analog channels, which must be preamplified, shaped, and digitized individually in current analog applications. In contrast to analog SiPM aggregates, a suited dSiPM technology does not suffer from an increased capacitance, which is a necessary trade-off for analog arrays of SiPMs. This results in maximized signal-to-noise independent from the total active surface. Additionally, a CMOS technology for the digitization of a SPAD signal can provide a finely tunable active cell quenching, detecting an avalanche in its early stages and promptly extinguishing it, with the possibility of completely turning off noisy or damaged cells. The ability to turn off individual pixels can greatly benefit overall DCR because a small subset of cells within a SiPM typically contribute disproportionately to the device's total dark noise [94, 96]. Moreover, with active cell quenching a programmable SPAD dead time can be implemented to greatly reduce the impact of delayed detrapping [97].

While it is possible to integrate both SPADs and CMOS circuitry on a single monolithic silicon device, this approach is constrained by current production techniques and is not cost-efficient, making it impractical for the large optical surfaces required in rare-event detectors. Current developments focus on what is known as 3D integration: (multi)layered, application-specific (ASIC), dense electronic boards coupled by micropads bonding to each SPAD in a suited SiPM. To achieve this, a special SiPM geometry is required for which SPAD outputs are not summed in an analog fashion but are vertically accessible via conductive channels in the silicon substrate (Through Silicon Vias, TSV). FBK recently developed a NUV/VUV front-side illuminated SiPM technology with TSV which permits single-SPAD readout via bonding pads on the backside of the device [98].

Finally, an intermediate ballistic step between analog SiPM readout and the digital SiPM may be that of pixelated SiPMs readout, i.e., front-end integrated readout and digitization of SiPM arrays with ASICs, with timing information provided by TDCs. An application of this technique can be envisioned as a DarkSide-20k-style tile of SiPMs with a fully digital output. While not possessing all of the benefits of dSiPMs, pixelated light readout would solve the most prominent problems of analog readout (high number of analog channels, difficulties in aggregating single-SiPM outputs) while resulting in a much more foreseeable technology based on already developed solutions and requiring a less extensive R&D [99]. This technology would be eventually outclassed by the cheap production of dSiPMs, providing a persuasive alternative up to that point.

The end goal of photon detection developments for large LAr detectors can be envisioned as a combination of the most advanced technologies presented in this section: a true photon-to-digital device with a large surface area, low power, low background, and high PDE in the VUV range and compliant to cryogenic temperatures.

4.3. Wavelength-Shifting and Xenon Doping

Despite the rapid advancements in vacuum ultraviolet- (VUV-)sensitive photon detection technologies, the photon detection efficiency within the VUV range has yet to achieve the performance already reached by such devices in the optical spectrum. Consequently, the most prominent method for detecting scintillation light in argon detectors continues to involve the use of wavelength-shifting materials (WLS), which absorb the light emitted by argon scintillation and subsequently reemit it at a wavelength closer to the optimal efficiency range of photon detectors, typically in the green or blue light spectrum. This is the case for numerous argon-based experiments across various research fields: dark matter searches (e.g., DEAP-3600, DarkSide-50), neutrino physics (e.g., ICARUS, MicroBooNE, SBN, DUNE), and neutrinoless double beta decay experiments (e.g., GERDA, LEGEND).

Many materials have already found use in LAr experiments, with some of the most popular choices being organic compounds such as 1,1,4,4-tetraphenyl-1,3-butadiene (TPB) [100], p-terphenyl [101], and polyethylene naphthalate (PEN) [102]. When choosing a WLS material to be used in an experiment, one has to consider the following: (i) performance, the most prominent characteristics desired in a wavelength-shifting material are high quantum yield (ratio of the number of reemitted photons to the number of absorbed photons), fast reemission time, and low overlap between emission and absorption spectra; (ii) scalability, the size of detectors has a great impact on the choice of wavelength shifters, given that the various coating techniques differ in scalability concerning both costs and practical considerations.

The most commonly used technique has been the vacuum evaporation of thin coatings of WLS, which can guarantee an exceptional uniformity of the substrate but becomes increasingly difficult for large surfaces making it unsuitable for large-scale implementation. Two alternatives are solvent coating [103, 104] and the use of WLS-doped polymeric matrices, which are easier to scale up as they do not require vacuum, but usually result in poorer quantum yield and uniformity. A promising result has been recently achieved with coatings of highly TPB-doped polystyrene, achieving better quantum yield than with TPB evaporation [100]. Finally, PEN can be laminated to produce large-area foils. An application with both TPB evaporation and PEN sheets was shown on a prototype TPC for the DUNE experiment [105].

A compelling avenue for wavelength shifting in future argon detectors involves the doping of argon with small amounts of xenon. The introduction of xenon has the notable effect of generating a scintillation at approximately 175 nm, a wavelength situated within a range where VUV photon detectors exhibit better performance than 128 nm. Beyond its impact on wavelength, xenon doping contributes to an overall improvement in scintillation, including an increased total scintillation yield, a reduction in attenuation length, enhanced resolution, and a decrease in the characteristic time of the long scintillation component. Remarkably, these advantageous effects are observable even with minimal xenon dopings $<$10 ppm) [106, 107, 108]. Recent measurements of the properties of Xe-doped Ar were carried out at the ProtoDUNE experiment at CERN, being the first large-scale prototype detector to test this technology [109, 110, 111].

For a more detailed exploration of the topic of wavelength-shifting materials, we defer to a comprehensive review authored by M. Kuzniak and A. M. Szelc [112].

5. CURRENT EXPERIMENTAL STATUS AND PROSPECTS

A collection of the most stringent limits for spin-independent DM-nucleon coherent scattering cross section is shown in Figure 5, with a focus on noble liquid detectors (xenon and argon experiments). Above a WIMP mass of $\sim$3 GeV/c^2, liquid xenon TPC experiments (XENONnT [115] and XENON1T [116], LZ [114], PandaX-II [117]) have placed the strongest constraints. The best limits for lower mass are from DarkSide-50 [15, 65] for the range (1–3) GeV/c^2 and CRESST-III [118], which uses a $CaWO_4$ crystal as the active medium, for even smaller masses. The light blue area represents the neutrino floor, which is the region in the WIMP parameter space where coherent elastic neutrino-nucleus scattering will statistically interfere with a WIMP measurement, strongly limiting the maximum sensitivity achievable by scaling the total exposure of an experiment [18, 22].

As shown in the plot, noble liquid TPCs are the leading technology for a large variety of dark matter particle candidates. These detectors still have room to improve their sensitivity before being limited by neutrino background. At the very ends of the mass interval allowed for a WIMP, sensitivity can be still improved by a factor of 10^2 by increasing the exposure while containing background to near zero levels. Scientists from the first-generation LAr dark matter projects (ArDM at LSC, DarkSide at LNGS, DEAP, and MiniCLEAN at SNOLAB) formed the Global Argon Dark Matter Collaboration (GADMC) [53] with the goal of pushing direct detection down to the neutrino floor. Similarly, the liquid xenon dark matter community united forces to realize a single multiton experiment, as proposed by the DARWIN collaboration [119] and now pursued by the XLZD consortium [120].

The argon experiments need to perform the largest step. The next experiment from the GADMC, DarkSide-20k, is currently in construction at LNGS and will cover and expand on the best current limits for high WIMP masses with a fiducial argon mass of about 20 tons. At the low-mass end, DarkSide-LowMass, with 1-ton argon dual-phase TPC adopting the S2-only operational mode, could improve over the current best limit set by DarkSide-50. R&D is still needed in order to abate the ER backgrounds, namely, develop more radiopure photosensors and demonstrate the ability to further deplete the ^{39}Ar in UAr (i.e., by isotopic separation).

The end goal of the GADMC is the realization of the Argo detector, aiming at 300 t fiducial mass, enough to achieve a sensitivity limit down to the neutrino floor for high WIMP masses. The detection sensitivity for WIMPs is anticipated to be primarily constrained by systematic uncertainties in nuclear recoil background resulting from coherent neutrino scattering of atmospheric neutrinos. Notably, the effective rejection of electronic recoil is expected to play a crucial role in mitigating background from solar neutrinos and residual internal backgrounds such as radon and its progeny. Projections from DarkSide-20k, DarkSide-LowMass, and Argo are reported as dashed lines in Figure 5.

In the following, details on the experimental setups (and results, when available) for current and future LAr dark matter direct detection experiments will be provided.

5.1. DarkSide-50

DarkSide-50 (DS-50) is an experiment by the DarkSide collaboration aimed at the direct detection of WIMPs using a two-phase argon TPC, located in the Laboratori Nazionali del Gran Sasso (LNGS). It ran from 2013 until 2020. The experimental apparatus consists of three nested detectors: a dual-phase LArTPC with a LAr mass of 46.4(7) kg (after position cuts), a 4.0 m-diameter Liquid Scintillator neutron Veto (LSV), and a 1 kt Water Cherenkov muon veto Detector (WCD).

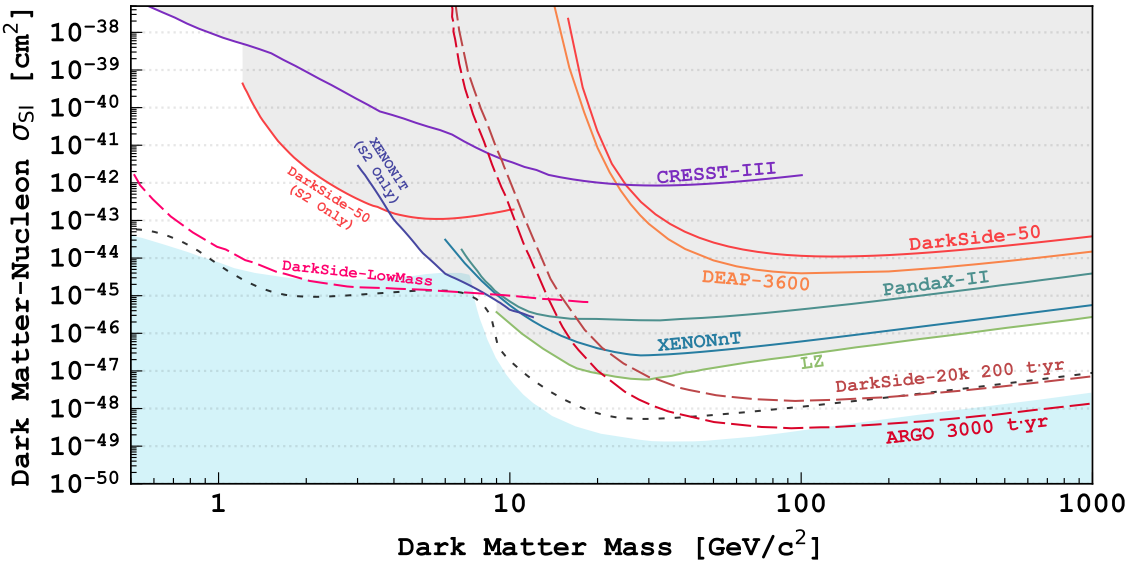

FIGURE 5: Exclusion limits from recent dark matter direct detection experiments and projections for future argon experiments. Argon experiments: DarkSide-50 (standard [15] and low-mass [65] analyses) and DEAP-3600 [113]. Xenon experiments: LZ [114], XENONnT [115], XENON1T (low-mass analysis) [116], and PandaX-II [117]. Other: CRESST-III [118]. Projections of future/proposed GADMC experiments (long-dashed lines): DarkSide-20k (200 t yr exposure), Argo (3000 t yr exposure), and DarkSide-LowMass [53]. The grey area represents the region of the WIMP parameter space collectively excluded. The light blue region represents the neutrino floor following the definition by Billard et al. [18, 22]; the short-dashed black line represents an alternative definition by O'Hare [19] as the cross-section values, depending on mass, below which the sensitivity loses its Poissonian scaling to background saturation. The curves corresponding to the two definitions of the neutrino floor are evaluated assuming an argon target.

The outermost veto detector, the Water Cherenkov Detector, is an 11 m tall cylinder filled with 1 kt of ultrapure water with the purpose of vetoing muon-induced events via detection of Cherenkov emission. Cherenkov light is picked up by 80 8″ PMTs, mounted on the walls and floor of the tank. The water also provides passive shielding against neutrons and gamma radiation from the surroundings of the experiment. Within it lies the Liquid Scintillator Veto, a vertically supported stainless steel sphere, 4 m in diameter, filled with a mixture of pseudocumene (1,2,4-trimethylbenzene), trimethyl borate and PPO (2,5-diphenyloxazole) wavelength shifter, equipped with 110 8″ PMTs with low-radioactivity glass bulbs and high-quantum-efficiency photocathodes. The LSV is designed to efficiently veto neutron interactions and provides further passive shielding to the LArTPC against external radiation; pioneered by DS-50, the concept of an active neutron veto is now widely spread among all present direct detection experiments.

At the core of the apparatus, the LArTPC is contained in a stainless steel cryostat inside the LSV. Its LAr active volume is enclosed by PTFE walls, mechanically smoothed to increase their reflectiveness. Electrodes for field generation consist of a thin layer of ITO deposited on two quartz windows, a metal wire grid, and copper rings surrounding the lateral walls to form the field-shaping cage. Two arrays of 19 3″ Hamamatsu PMTs are placed behind the windows looking toward the active region. To accommodate for the spectral response of the PMTs, all inner surfaces of the detector (including the two quartz windows) are covered by a thin evaporation of TPB. Gas argon is produced and maintained by a resistive boiler on the external wall of the TPC, connected to the internal region. A picture of the LArTPC of DS-50 is presented in Figure 6(a).

DS-50 published in 2018 the best exclusion limits with an argon detector at the time of publication, from 532.4 live days of blinded data, achieving a total of zero background [15]. On the low-mass spectrum, DS-50 currently holds the most stringent limits to date for WIMP masses in the range (1–3) GeV/c^2 [65] obtained with a threshold of 0.6 keV for nuclear recoils (0.06 keV ER-equivalent) with an S2-only analysis.

5.2. DEAP-3600

DEAP-3600 is a direct detection experiment based on an LAr scintillation detector, still running as of 2024, set at SNOLAB in an underground facility 2 km underground. The active volume is defined by a 5-cm-thick spherical ultrapure acrylic vessel, internally coated with TPB, containing about 3200 kg of atmospheric argon viewed by 255 8″ high-quantum-efficiency PMTs. The PMTs are connected to the vessel via acrylic light guides which together with polyethylene filler blocks provide neutron shielding and thermal insulation. The vessel is placed in a stainless steel shell, which, in turn, is submerged in a cylindrical tank filled with ultrapure water and instrumented with 48 PMTs to serve as a muon veto. A picture is in Figure 6(b).

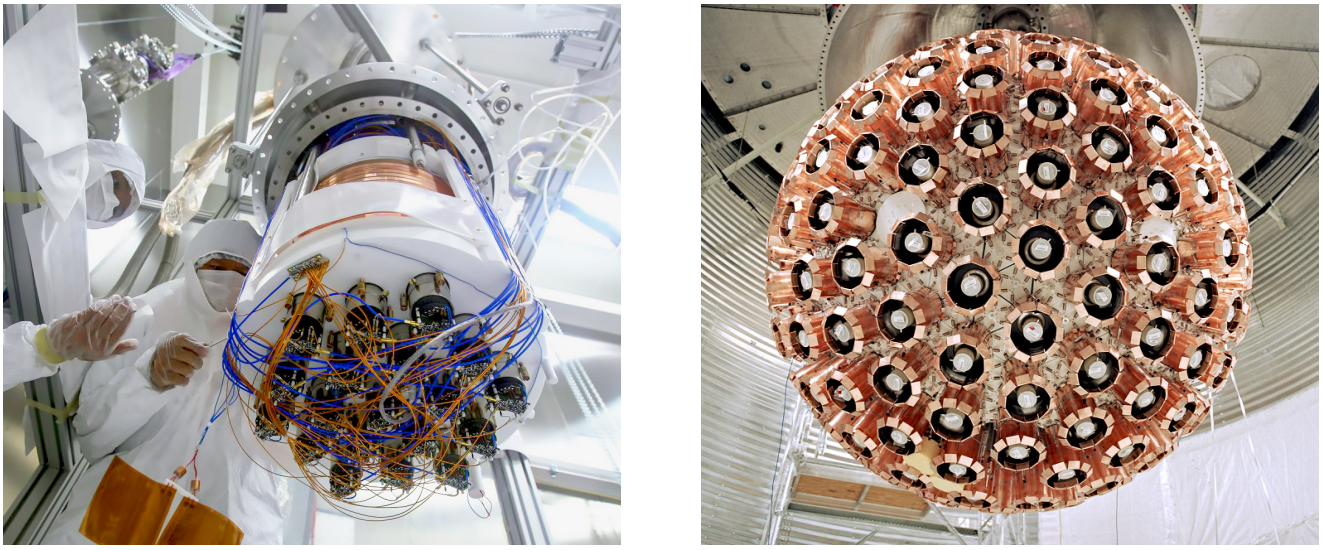

(a) (b)

FIGURE 6: (a) The LArTPC of DarkSide-50 seen from below. Picture from [121]. (b) The scintillation detector of EAP-3600. PMTs are visible facing the inner volume of the detector, with copper shields to reduce the thermal gradients across them. Picture from [122].

The experiment reached very low levels of radon background (0.15 μBq/kg). This result could be achieved by developing a controlled acrylic production chain and by "resurfacing" the acrylic vessel to remove the inner surface layer exposed to radon during construction.

The last results from DEAP-3600 were published in 2019 for a spin-independent WIMP interaction, obtaining an exclusion limit for the 90% CL and a WIMP of mass 100 GeV/c^2 of 3.9×10^{-45} cm^2 [113]. The same data was used to constrain cross section for Planck-scale particle dark matter [123]. Other notable contributions from the collaboration include extensive work on modeling the argon pulse shape with DEAP-3600 setup, including a delayed $\mathcal{O}(1\,\mathrm{ms})$ emission by TPB [124] and characterizing different PSD parameters using ^{39}Ar data [45], for which a precision measurement of activity in atmospheric argon was very recently published [125].

5.3. *DarkSide-20k*

DarkSide-20k (DS-20k) is the experiment designed by the GADMC to improve the limits set by DarkSide-50 and DEAP-3600 of more than a factor 10^3 for a 100 GeV/c^2 WIMP. The experiment is in the construction phase at the LNGS underground laboratories. It will use a two-phase argon TPC with an active mass of 51 t (fiducial mass of 20 t) to reach an exposure of 200 t · yr while maintaining a negligible background level of $<$0.1 background events, excluding neutrino background, in the WIMP region of interest [127].

The main innovations of the DS-20k detector are a membrane cryostat enclosing both the outer veto and the inner detector, an optical readout based on large-area radiopure cryogenic SiPMs photon counters for both the TPC and veto system; the use of gadolinium doped acrylic for the TPC walls to reduce encumbrance of the neutron veto system; and the use of radiopure UAr for both the neutron veto and LArTPC. A scheme of the experiment is presented in Figure 7(a).

The DS-20k cryostat will be a ProtoDUNE-like membrane cryostat [128, 129] with an approximately cubical shape and an internal volume of about 580 m^3. It will be filled with atmospheric liquefied argon, serving as the outer veto detector medium and thermal bath for the inner detector. The inner detector is located in the central volume of the DS-20k cryostat, enclosed by a stainless steel vessel. It is comprised of the inner veto and the TPC. The two systems are conjoined, as the walls of the TPC are made of 15-cm-thick slabs of Gd-infused PMMA [130]: Gd serves as a neutron-capture material, emitting several gammas after absorption of a thermalized neutron, which can then be detected in the inner veto for neutron tagging, with an inefficiency of 10^{-6}. The working principle of the veto system is illustrated in Figure 7(b). With this choice, the veto system is compact enough to be entirely submerged in low-radioactivity argon together with the TPC, at a slight over-pressure with respect to atmospheric pressure [127]. The TPC itself is shaped as a regular octagonal prism with an inscribed circle diameter and height of 350 cm. The eight lateral walls are internally covered with a sheet of Vikuiti ESR. The octagonal volume is capped by two transparent acrylic windows that contain both the liquid argon region and the gas pocket. Most conductive elements for generating the electric field are made of thin films of Clevios, a conducting polymer applied to the transparent windows at the top and bottom to form the anode and cathode and on the walls of the TPC to create the field-shaping cage. The grid for field decoupling and electron extraction is instead made by an array of parallel, stainless steel wires. Inside the TPC, all surfaces are deposited with a TPB wavelength shifter to convert the scintillation light of argon to light with a wavelength of 420 nm.

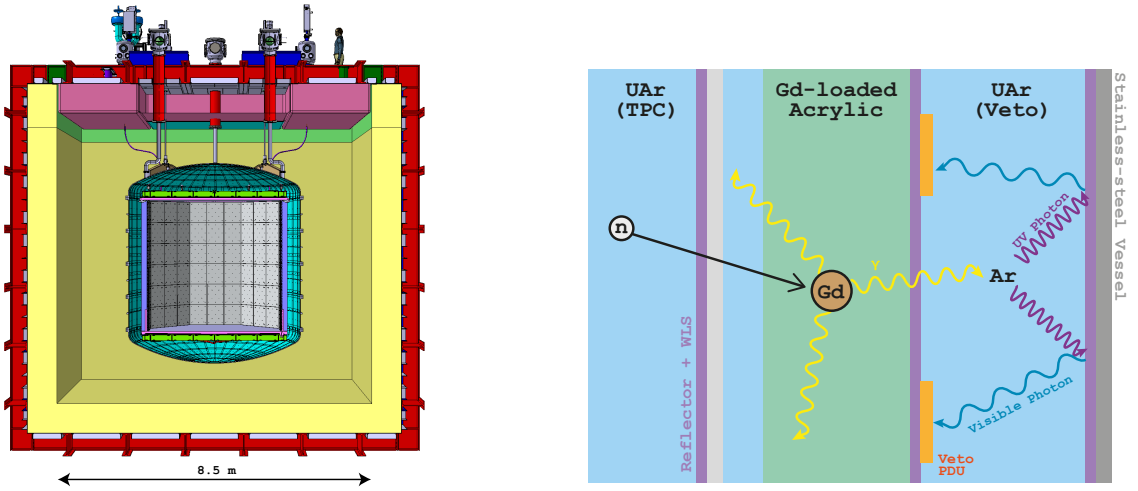

(a) (b)

FIGURE 7: (a) Front view of the DarkSide-20k detector, showcasing its components. The membrane cryostat, colored red and yellow, houses the inner detector submerged in atmospheric liquid argon. The stainless steel vessel, depicted in light blue, contains the TPC structure and the veto and is filled instead with ultrapure argon. The TPC is visible as the central octagon, enclosed by its walls and caps (green blocks) which are made of Gd-loaded PMMA. Figure reprinted from [126]. (b) Scheme of the inner veto system of DS-20k. Neutrons thermalize in the walls of the TPC and are captured by gadolinium, releasing several gammas detectable in the veto UAr volume, instrumented with PDUs.

In DS-20k, the light readout for both TPC and veto systems will be based on the modular photosensor unit Photon Detection Unit (PDU) described in Section 4.2.3. In the TPC, two planes of PDUs with 100% coverage will constitute the optical readout for a total of 2112 independent readout channels, totaling a surface of about 21 m^2. For the veto system, a slightly different PDU with the same dimensions, but featuring an ASIC preamplifier instead of the TPC PDU TIA, will be used for optical readout, for a total of 120 channels and an active surface of about 5 m^2 [126]. TPC PDUs will be assembled at the Nuova Officina Assergi (NOA) production facility at the Laboratori Nazionali del Gran Sasso, Italy. NOA features a 420 m^2 ISO6 cleanroom fully equipped with commercial and custom-designed machinery for SiPM tiles and electronics integration in an adequate radio-controlled infrastructure capable of both mass production and cryogenic testing.

Due to the scale of DS-20k, the use of atmospheric argon in the TPC would pile up the detector by the frequent emissions from ^{39}Ar. Hence, the inner detector will be filled with radiopure argon extracted from the same underground CO_2 well which was discovered to possess a radioactivity by ^{39}Ar reduced of a 1400-fold factor with respect to AAr, as measured by DarkSide-50 [51]. The extraction, purification, and transportation of such large quantities from underground sources is a major technical challenge which requires careful planning and industrial infrastructure. To this purpose, the DarkSide collaboration established the Urania and Aria projects which will ensure the procurement of the necessary UAr at the desired level of purity and radiopurity, as well as provide an industrial infrastructure for the procurement of low-radioactivity argon for future larger experiments.

Urania will extract and purify the underground argon from the CO_2 wells at the Kinder Morgan Doe Canyon Facility, located in Cortez, CO. The extraction site is the same from which the UAr used in the DarkSide-50 experiment was extracted. The well stream is made up mainly of CO_2 with an UAr content of 430 ppm, and it is fed to three gas-processing units used for the separation of UAr, followed by a purification system optimized for the feed composition to achieve a UAr purity better than 99.99%. The maximum extraction rate will be 330 kg/d. From Urania, the UAr is shipped to the Aria facility [131], in Sardinia, for further chemical purification. The facility consists of a 350 m tall cryogenic distillation column installed in a vertical shaft located in the Seruci mine. Aria will reduce chemical impurities in UAr by a factor of more than 10^3 per pass, at a rate of $\mathcal{O}(1\,\mathrm{t/d})$. Although at a much lower rate, Aria is also capable of separating isotopes by cryogenic distillation and further depleting the radioactive ^{39}Ar component. The first successful test of isotopic separation in the Aria prototype is reported in [132]. The measurement of the ^{39}Ar abundance in batches of the UAr produced by Urania and Aria will be carried out by the DArT in the ArDM experiment at Laboratorio Subterraneo de Canfrac (LSC), Spain, which aims at measuring ^{39}Ar depletion factors of the order of 1000 with 10% precision [133]. The experimental setup is a single-phase liquid argon detector with an active volume of about 1 L. Air transport is avoided to reduce the cosmogenic activation of the UAr during transport. The estimated exposure time due to shipping is 134 days, and different locations and altitudes are considered to extract a measurement of cosmogenic activation, resulting in increased activity of 0.0190(16) mBq/kg, which is 2.6% of the activity measured in DarkSide-50 for UAr [134].

5.4. DarkSide-LowMass

In a two-phase LArTPC, photon collection faces an unavoidable efficiency loss (down to a fraction of the total scintillation light) caused by the quantum efficiency of photon counters and suboptimal light guiding; moreover, photon reconstruction must contend

with noise. On the other hand, the achievable electron lifetimes, combined with excellent extraction efficiency as well as the highly advantageous charge-to-light conversion factor from electroluminescence, result in almost 100% efficiency in electron counting. Consequently, the ionization channel is capable of accessing energies closer to the work function, much lower than those achieved by scintillation alone, albeit in a nonbackground-free regime. Many experiments using noble liquids TPCs have published constraints on light-dark matter by exploiting the lower threshold achievable by an S2-only analysis. Argon is particularly appealing for a light-dark matter dedicated detector due to its relatively light nucleus, which favors higher-energy recoils from light-dark matter due to an increased kinematic coupling.

DarkSide-LowMass is a planned experiment by the GADMC aiming at developing such a highly-optimized detector by focusing on enhancing $S2$ and minimizing backgrounds that generate signals at the keV scale [66] through a 1 t yr exposure experiment, conceptually similar to an upscaled DS-50, incorporating many of the innovations of DS-20k and low-radioactivity UAr with further suppression of ^{39}Ar achieved through isotopic distillation by Aria. With respect to DS-50, a more stringent fiducialization is envisioned which includes a buffer veto for photon detector-induced background, to effectively mitigate low-energy γ-rays. Projections for a possible detector design are included in Figure 5.

5.5. Argo

The GADMC's long-term goal is the construction of the Argo detector, which will feature a 300 t fiducial mass and a target exposure of several thousand t yr [135, 136]. This aims to elevate experimental sensitivity to the point where coherent scattering of atmospheric neutrinos becomes the background limitation in WIMP searches. The Urania plant and Aria facility's throughput will extract and purify 400 t of ultrapure argon over approximately 4 years. Due to the very large optical coverage required for Argo (of the order of 100 m^2), further developments in photo-electronics, continuing the R&D work of DS-20k, would greatly simplify the construction of the experiment. The next anticipated breakthrough is that of implementing either low-power front-end digitization on a PDU-like photon detector or fully digital SiPMs. Such a development would significantly reduce costs associated with cabling and management of analog systems, improving spatial resolution and also positively impacting noise and total background of the detector.

The high target mass and low-energy threshold combined with background mitigation strategies employed for dark matter detection will make Argo versatile and sensitive enough to measure astrophysical ultrarare neutrino fluxes with high resolution. Argo will be capable of measuring both hep neutrinos and CNO neutrinos; a measurement of CNO flux would sort out the "Solar Metallicity Problem" [53], as 3500–5000 CNO neutrino interactions are expected for an exposure of 1500 t yr, with the total interactions depending on the metallicity model [137, 138]. Moreover, Argo would be able to measure neutrinos from core-collapse supernovae via the coherent elastic neutrino-nucleus flavor-blind channel, providing a measurement for the total unoscillated flux and being able to detect a supernova signal (for an 11 $M_\odot$ star) with 5σ significance up to 25 kpc from Earth, well beyond the edges of the Milky Way [139].

5.6. Developments for Dark Matter Studies in DUNE

The Deep Underground Neutrino Experiment (DUNE) aims at investigating long-baseline neutrino oscillations on accelerator-produced neutrinos. The experiment will perform precision measurements of oscillation parameters, explore the neutrino mass hierarchy, and investigate CP-violation within the leptonic sector. Additionally, DUNE is also sensitive to astrophysical neutrinos, providing insights into physics beyond the standard model and a high-statistics measurement of supernova neutrino bursts (SNBs).

The far detector consists of four modules, each being an LArTPC with an active target of 17 kilotons of liquid argon, for a total fiducial mass (over four modules) of 40 kt [78]. This huge detector complex will be located 1.5 km underground at the Sanford Underground Research Facility (SURF) in South Dakota. Out of the four modules of the far detector, the first two are single-phase LArTPCs with either horizontal or vertical drift directions. The Horizontal Drift (HD) module is separated into four drift volumes of 3.5 m $\times$ 12 m $\times$ 58 m each, by alternating anode and cathode planes [105]. The ionization electrons produced during an event drift horizontally and are recorded on the vertical Anode Plane Assemblies (APA). The APA consists of three sets of wires oriented at different angles, with a 5 mm wire spacing chosen for optimal spatial resolution and signal-to-noise ratio. The drift length is 3.5 m. The vertical drift (VD) module is designed as a single-phase LArTPC with electron drift along the vertical axis [140]. It consists of two volumes with dimensions of 13.5 m $\times$ 6.5 m $\times$ 60 m, separated by a cathodic plane located at the midpoint in height. In this module, the ionization charge will be collected by two anode planes positioned at the top and bottom of the module, constructed using stacked layers of perforated PCBs equipped with electrode strips to collect the drifting electrons.

In both modules, scintillation light is read out by large photon detectors based on a technology known as X-Arapuca [141]. The X-Arapuca technology is composed of a box with highly reflective internal surfaces and one or two acceptance windows.These windows consist of a shortpass dichroic filter (400 nm cutoff) that is coated with pTP, which converts VUV light to 350 nm light, below the cutoff wavelength of the filter. This conversion allows the photons to pass through the filter. Inside the X-Arapuca box, there is an acrylic slab embedding a different WLS compound. This compound serves to convert the photons back to a wavelength above the cutoff point of the filter so that the filter is reflective of converted photons. As a result, photons are trapped inside the highly reflective box and can then be detected by SiPMs installed on the internal lateral walls. The X-Arapuca technology is adopted for the Photon Detection Systems of both HD and VD modules.

The last two modules of DUNE are programmed as a later upgrade of the experiment (DUNE Phase II), with the third module anticipated to be an improved VD. The specifications for the fourth module remain instead undetermined, and inputs from the community are being received for an innovative module capable of extending DUNE's physics reach. As such, the name given to the fourth module is Module of Opportunity (MoO). The US P5 Particle Physics Project Prioritization Panel recently released

recommendations to proceed with full R&D for the MoO [142]. Among the proposed technologies, the most interesting ones aim at expanding the physics reach by lowering the background and reducing the energy threshold, projected to be (5–10) MeV for the first two modules, to the range of 100 keV and below.

The easiest step for reducing the threshold is to enhance light collection by increasing optical coverage and collection efficiency. X-Arapuca modules, while being characterized by a large surface area, have a collection efficiency of a few percent, which is not an issue for physics above the MeV scale. An alternative route could be the employment of enhanced light guiding provided by metalenses, flat optical components which can mimic the functions of conventional lenses [143] and be mass produced for cost abatement. They could find use in systems with limited optical coverage to focalize scintillation light, enhancing the global photon-collection efficiency [144].

Enhancements in the field of charge collection are also viable for reducing the detector's threshold. Pixelated charge readout is a promising technology capable of doing so, also improving spatial resolution and imaging capabilities, by front-end processing and digitization of dense arrays of charge collection pads: two current developments are the Q-Pix [145, 146] and LArPix [147] technologies. The Q-Pix is based on a continuously integrating low-power charge amplifier coupled to a Schmitt trigger, with charge information extracted from the reset rate of the trigger. LArPix uses instead low-power ASIC front-end electronics for self-triggering, amplification, digitization, and multiplexed readout. These devices may be then coupled to a light-charge hybrid readout system, with two possible trajectories being either (i) the independent measurement of charge and light in a monolithic tile as proposed by SoLAr [148], which combines anodic pads and (VUV) SiPMs on a single multilayered PCB or (ii) the simultaneous readout of light and charge in multimodal pixels, converting light to charge via thin-film photosensitive coatings (e.g., amorphous selenium) [149, 150]. The minimum threshold for these devices is mainly limited by electronic noise, and it appears to be extremely unlikely for charge collection devices to become sensitive below several hundred electrons ($\mathcal{O}(100\,\mathrm{keV})$) without any form of charge amplification, excluding WIMP direct detection from their available physics scope, at least without a significant breakthrough.

Charge amplification by electroluminescence provides an excellent channel for detecting even a single electron with unmatched efficiency, as discussed throughout this review. However, the two-phase paradigm, in the form of the dual-phase LArTPC, will prove to be a challenge to scale up because of the difficulties in stabilizing a thin gas layer over surfaces of a hundred or more square meters. A few designs for combined charge and light amplification are being developed which make use of GEMs or GEM-like technology to produce electroluminescence in gas with more forgiving requirements for gas-pocket stability with respect to the original two-phase TPC. A small perturbation to the LArTPC is the Cryogenic Avalanche Detector, whose design envisions SiPM-based readout and one or more planes of thick GEMs (THGEMs) directly placed in a suitable gas layer [151, 152]. Based on the same concept, the ARIADNE program employs glass THGEMs for charge-to-light conversion in a double-phase LArTPC, with fast photon-counting camera optical readout based on the TimePix pixelated photosensor and achieving exceptional imaging capabilities with a warm, easily upscalable device, intrinsically decoupled from the electronic noise of the detector [153, 154, 155, 156]. Finally, Liquid Hole Multipliers (LHMs) are charge amplifiers that could be used directly in liquid argon [157], assisted by gas bubbles created with heating wires and trapped under a (TH)GEM by surface tension [158, 159]. To detect light, LHMs can make use of photo-conductive films for light-to-charge conversion, followed by charge amplification.

The ongoing R&D efforts will bring forth enhanced capabilities, enabling the detection of BSM physics or dark matter signatures beyond the primary objectives of the experiment. DUNE will be able to conduct dark matter searches for models that predict energetic interaction at the MeV scale. An example is boosted dark matter models, for which (part of) the dark sector has received a Lorentz boost [160]. Strategies for the detection of boosted dark matter and other exotic models are still under discussion [161, 162].

Sensitivity to WIMPs becomes competitive in DUNE if the energy threshold can be reduced to below 100 keV while significantly improving radioactive backgrounds. A dedicated design for a low background module considers a reenvisioning of the VD module, with the addition of an optically isolated inner volume, defined by ultrapure acrylic walls and instrumented with DarkSide-20k style SiPM photosensors [54]. A high photosensor coverage, the use of underground argon, a water shield, an accurate material choice, and fiducialization down to a volume of 2 kt are the key modifications to the original design of the VD module needed to lower the threshold for nuclear recoils below the 100 keV scale. Such a module would be sensitive to WIMP dark matter, coherent elastic neutrino-nucleus scattering from supernovae neutrinos and $0\nu\beta\beta$ decay via Xe-doping [163].

6. CONCLUSIONS

In the hunt for the WIMP, the two-phase LArTPC has demonstrated with full marks to be a versatile and powerful detector; the excellent properties of argon as a detector medium make it potentially scalable by at least three orders in magnitude in mass with respect to current experiments. This detector technology will likely lead the scene of dark matter searches with LAr down to the neutrino floor over a WIMP mass range spanning more than four orders of magnitude. The use of a sophisticated active veto system, ^{39}Ar depleted underground argon, and radiopure materials, combined with the unique scintillation properties of argon, will enable future LAr experiments to maintain a negligible instrumental background, resulting in maximum sensitivity achievable with a given exposure. However, this may be only possible with a parallel effort in the development of cheap, scalable, radiopure readout technologies and the prompt procurement of large volumes of radiopure argon. The Global Argon Dark Matter Collaboration is currently devoting unparalleled efforts on both subjects, from R&D processes to full industrial production for Si-based large-surface photon counters and, simultaneously, extraction and purification of underground argon with reduced ^{39}Ar content. DarkSide-20k is the next LAr experiment joining the race to the neutrino floor, currently in construction at the LNGS underground laboratories. The full GADMC experimental program is expected to fulfill its physics goals in about two decades.

As technology progresses, future detectors may find a great advantage in adopting alternative light, charge, or hybrid readout technologies. On the luminous side, the holy grail of photon detection development in the field of LAr detectors can be envisioned as a cheap VUV-sensitive monolithic photon-to-digital converter, capable of enormously reducing the complexity of current detectors by dropping the requirements for WLSs and many-channel analog readout, while also solving some of the nuisances associated with SiPMs. It is highly probable that, beyond the next generation of detectors, the current two-phase design will require adaptations or be abandoned altogether due to challenges associated with stabilizing a thin gaseous layer in large-scale detectors. Parallel to the development of light detection, novel technologies capable of providing stable, reliable, and ultralow threshold readout for the ionization signal may provide a compelling alternative to the dual phase, ideally fully integrating light and charge-readout systems.

Finally, an enriching perspective for the field of dark matter detection would be empowering DUNE by designing a Module of Opportunity sensitive to energies of $\mathcal{O}(100\,\mathrm{keV})$, making DUNE MoO the biggest yet-envisioned WIMP detector. The feasibility of this project will become clearer as current readout developments steadily progress toward industrial readiness. Independently from the chosen technology, a detector with the size of one of the DUNE modules would plunge deep below the neutrino floor, posing a great limit to the maximum achievable sensitivity as the detector would be engulfed by the neutrino background. This may be circumvented with an extra discrimination step based on the signatures of the WIMP and neutrino fluxes, as their interaction is indistinguishable from the signal they generate in argon.

CONFLICTS OF INTEREST

The authors declare that there are no conflicts of interest regarding the publication of this paper.

References

[1] J. Billard et al. Direct detection of dark matter - APPEC committee report. *Rep. Prog. Phys.*, 85(5):056201, May 2022.
[2] S. D. McDermott et al. Turning off the lights: How dark is dark matter? *Phys. Rev. D*, 83(6):063509, 2011.
[3] B. Audren et al. Strongest model-independent bound on the lifetime of Dark Matter. *JCAP*, 12(12):028, December 2014.
[4] V. Springel et al. The large-scale structure of the Universe. *Nature*, 440(7088):1137–1144, April 2006.
[5] N. Aghanim et al. *Planck* 2018 results: I. Overview and the cosmological legacy of *Planck*. *Astron. Astrophys.*, 641:A1, September 2020.
[6] N. Aghanim et al. *Planck* 2018 results: VI. Cosmological parameters. *Astron. Astrophys.*, 641:A6, September 2020.
[7] G. Steigman et al. Precise relic WIMP abundance and its impact on searches for dark matter annihilation. *Phys. Rev. D*, 86(2):023506, July 2012.
[8] Y. You et al. Signatures and detection prospects for sub-GeV dark matter with superfluid helium. *J. High Energ. Phys.*, 2023(7):9, July 2023.
[9] B. Von Krosigk et al. DELight: A Direct search Experiment for Light dark matter with superfluid helium. *SciPost Phys. Proc.*, (12):016, July 2023.
[10] R. Anthony-Petersen et al. Applying Superfluid Helium to Light Dark Matter Searches: Demonstration of the HeRALD Detector Concept, July 2023.
[11] D. Baxter et al. Recommended conventions for reporting results from direct dark matter searches. *Eur. Phys. J. C*, 81(10):907, October 2021.
[12] J. Lewin and P. Smith. Review of mathematics, numerical factors, and corrections for dark matter experiments based on elastic nuclear recoil. *Astropart. Phys.*, 6(1):87–112, 1996.
[13] D. N. Spergel. Motion of the Earth and the detection of weakly interacting massive particles. *Phys. Rev. D*, 37(6):1353, 1988.
[14] G. J. Feldman and R. D. Cousins. Unified approach to the classical statistical analysis of small signals. *Phys. Rev. D*, 57(7):3873–3889, April 1998.
[15] P. Agnes et al. DarkSide-50 532-day dark matter search with low-radioactivity argon. *Phys. Rev. D*, 98(10):102006, November 2018.
[16] G. Heusser. Low-Radioactivity Background Techniques. *Annu. Rev. Nucl. Part. Sci.*, 45(1):543–590, December 1995.
[17] D. Akimov et al. Observation of coherent elastic neutrino-nucleus scattering. *Science*, 357(6356):1123–1126, 2017.
[18] J. Billard et al. Implication of neutrino backgrounds on the reach of next generation dark matter direct detection experiments. *Phys. Rev. D*, 89(2):023524, January 2014.
[19] C. A. J. O'Hare. New Definition of the Neutrino Floor for Direct Dark Matter Searches. *Phys. Rev. Lett.*, 127(25):251802, December 2021.
[20] J. H. Davis. Dark matter vs. neutrinos: The effect of astrophysical uncertainties and timing information on the neutrino floor. *J. Cosmol. Astropart. Phys.*, 2015(03):012, March 2015.
[21] S. Sassi et al. Solar neutrinos and dark matter detection with diurnal modulation. *Phys. Rev. D*, 104(6):063037, September 2021.
[22] F. Ruppin et al. Complementarity of dark matter detectors in light of the neutrino background. *Phys. Rev. D*, 90(8):083510, October 2014.
[23] C. A. J. O'Hare et al. Readout strategies for directional dark matter detection beyond the neutrino background. *Phys. Rev. D*, 92(6):063518, September 2015.
[24] F. Mayet et al. A review of the discovery reach of directional Dark Matter detection. *Physics Reports*, 627:1–49, April 2016.
[25] Brookhaven National Laboratory (BNL). Liquid Argon Properties (Tables and Calculators).
[26] C. Rubbia. The liquid argon time projection chamber: A new concept for neutrino detectors. CERN-EP-INT-77-8 CERN-EP-INT-77-08, CERN, May 1977.
[27] W. H. Lippincott et al. Scintillation time dependence and pulse shape discrimination in liquid argon. *Phys. Rev. C*, 78(3):035801, September 2008.
[28] P.-A. Amaudruz et al. Measurement of the scintillation time spectra and pulse-shape discrimination of low-energy β and nuclear recoils in liquid argon with DEAP-1. *Astroparticle Physics*, 85:1–23, December 2016.
[29] M. Boulay and A. Hime. Technique for direct detection of weakly interacting massive particles using scintillation time discrimination in liquid argon. *Astroparticle Physics*, 25(3):179–182, April 2006.
[30] P. Agnes et al. Performance of the ReD TPC, a novel double-phase LAr detector with silicon photomultiplier readout. *Eur. Phys. J. C*, 81(11):1014, November 2021.

[31] T. Doke et al. Scintillation yields by relativistic heavy ions and the relation between ionization and scintillation in liquid argon. *Nuclear Instruments and Methods in Physics Research Section A: Accelerators, Spectrometers, Detectors and Associated Equipment*, 235(1):136–141, March 1985.

[32] T. Doke et al. Absolute Scintillation Yields in Liquid Argon and Xenon for Various Particles. *Jpn. J. Appl. Phys.*, 41(Part 1, No. 3A):1538–1545, March 2002.

[33] T. Doke. *Fundamental Properties Of Liquid Argon, Krypton And Xenon As Radiation Detector Media*, volume Experimental Techniques in High-Energy Nuclear and Particle Physics, pp. 537–577. World Scientific, 2 edition, November 1991.

[34] E. Conti et al. Correlated fluctuations between luminescence and ionization in liquid xenon. *Phys. Rev. B*, 68(5):054201, August 2003.

[35] Lindhard, J et al. Integral Equations Governing Radiation Effects. (Notes On Atomic Collisions, III). *Kgl. Danske Videnskab., Selskab. Mat. Fys. Medd.*, 33(10), 1963.

[36] D.-M. Mei et al. A model of nuclear recoil scintillation efficiency in noble liquids. *Astroparticle Physics*, 30(1):12–17, August 2008.

[37] J. B. Birks. Scintillations from Organic Crystals: Specific Fluorescence and Relative Response to Different Radiations. *Proc. Phys. Soc. A*, 64(10):874–877, October 1951.

[38] H. Cao et al. Measurement of scintillation and ionization yield and scintillation pulse shape from nuclear recoils in liquid argon. *Phys. Rev. D*, 91(9):092007, May 2015.

[39] G. Jaffé. Zur Theorie der Ionisation in Kolonnen. *Annalen der Physik*, 347(12):303–344, January 1913.

[40] J. Thomas and D. A. Imel. Recombination of electron-ion pairs in liquid argon and liquid xenon. *Phys. Rev. A*, 36(2):614–616, July 1987.

[41] V. Cataudella et al. Directional modulation of electron-ion pairs recombination in liquid argon. *J. Inst.*, 12(12):P12002, December 2017.

[42] DarkSide-20k Collaboration et al. Constraints on directionality effect of nuclear recoils in a liquid argon time projection chamber. *Eur. Phys. J. C*, 84(1):24, January 2024.

[43] P. Agnes et al. CALIS—A CALibration Insertion System for the DarkSide-50 dark matter search experiment. *J. Inst.*, 12(12):T12004, December 2017.

[44] P. Agnes et al. First results from the DarkSide-50 dark matter experiment at Laboratori Nazionali del Gran Sasso. *Physics Letters B*, 743:456–466, April 2015.

[45] P. Adhikari et al. Pulse-shape discrimination against low-energy Ar-39 beta decays in liquid argon with 4.5 tonne-years of DEAP-3600 data. *Eur. Phys. J. C*, 81(9):823, September 2021.

[46] P. Benetti et al. Measurement of the specific activity of 39Ar in natural argon. *Nuclear Instruments and Methods in Physics Research Section A: Accelerators, Spectrometers, Detectors and Associated Equipment*, 574(1):83–88, April 2007.

[47] H. Loosli. A dating method with 39Ar. *Earth and Planetary Science Letters*, 63(1):51–62, April 1983.

[48] T. Lyubetskaya and J. Korenaga. Chemical composition of Earth's primitive mantle and its variance: 1. Method and results. *J. Geophys. Res.*, 112(B3):2005JB004223, March 2007.

[49] D. Acosta-Kane et al. Discovery of underground argon with low level of radioactive 39Ar and possible applications to WIMP dark matter detectors. *Nuclear Instruments and Methods in Physics Research Section A: Accelerators, Spectrometers, Detectors and Associated Equipment*, 587(1):46–51, March 2008.

[50] J. Xu et al. A study of the trace 39Ar content in argon from deep underground sources. *Astroparticle Physics*, 66:53–60, June 2015.

[51] P. Agnes et al. Results from the first use of low radioactivity argon in a dark matter search. *Phys. Rev. D*, 93(8):081101, April 2016.

[52] C. E. Aalseth et al. DarkSide-20k: A 20 tonne two-phase LAr TPC for direct dark matter detection at LNGS. *Eur. Phys. J. Plus*, 133(3):131, March 2018.

[53] GADMC. Future Dark Matter Searches with Low-Radioactivity Argon. In *European Particle Physics Strategy Update 2018 – 2020*, January 2018.

[54] A. Avasthi et al. Low Background kTon-Scale Liquid Argon Time Projection Chambers. *arXiv*, 2203.08821, 2022.

[55] T. Alexander et al. The Low-Radioactivity Underground Argon Workshop: A workshop synopsis. *arXiv*, 1901.10108, 2019.

[56] COHERENT Collaboration et al. Applications for Underground Argon - Snowmass 2021, 2021.

[57] D. Akimov et al. First Measurement of Coherent Elastic Neutrino-Nucleus Scattering on Argon. *Phys. Rev. Lett.*, 126(1):012002, January 2021.

[58] N. Abgrall et al. The large enriched germanium experiment for neutrinoless double beta decay (LEGEND). In *Workshop On Calculation Of Double-beta-decay Matrix Elements (Medex'17)*, Prague, Czech Republic, 2017.

[59] LEGEND Collaboration et al. LEGEND-1000 Preconceptual Design Report. *arXiv*, 2107.11462, 2021.

[60] P. Agnes et al. Constraints on Sub-GeV Dark-Matter–Electron Scattering from the DarkSide-50 Experiment. *Phys. Rev. Lett.*, 121(11):111303, September 2018.

[61] P. Agnes et al. Low-Mass Dark Matter Search with the DarkSide-50 Experiment. *Phys. Rev. Lett.*, 121(8):081307, August 2018.

[62] P. Agnes et al. Search for low mass dark matter in DarkSide-50: The bayesian network approach. *Eur. Phys. J. C*, 83(4):322, April 2023.

[63] P. Agnes et al. Search for Dark-Matter–Nucleon Interactions via Migdal Effect with DarkSide-50. *Phys. Rev. Lett.*, 130(10):101001, March 2023.

[64] P. Agnes et al. Search for Dark Matter Particle Interactions with Electron Final States with DarkSide-50. *Phys. Rev. Lett.*, 130(10):101002, March 2023.

[65] P. Agnes et al. Search for low-mass dark matter WIMPs with 12 ton-day exposure of DarkSide-50. *Phys. Rev. D*, 107(6):063001, March 2023.

[66] P. Agnes et al. Sensitivity projections for a dual-phase argon TPC optimized for light dark matter searches through the ionization channel. *Phys. Rev. D*, 107(11):112006, June 2023.

[67] E. Alfonso-Pita et al. Snowmass 2021 Scintillating Bubble Chambers: Liquid-noble Bubble Chambers for Dark Matter and CEνNS Detection. *arXiv*, 2207.12400, 2022.

[68] C. Amole et al. Data-driven modeling of electron recoil nucleation in PICO C 3 F 8 bubble chambers. *Phys. Rev. D*, 100(8):082006, October 2019.

[69] B. Broerman. The Scintillating Bubble Chamber Experiment. *SciPost Phys. Proc.*, 023(12), July 2023.

[70] D. Baxter et al. First Demonstration of a Scintillating Xenon Bubble Chamber for Detecting Dark Matter and Coherent Elastic Neutrino-Nucleus Scattering. *Phys. Rev. Lett.*, 118(23):231301, June 2017.

[71] K. Nakamura et al. Latest bialkali photocathode with ultra high sensitivity. *Nuclear Instruments and Methods in Physics Research Section A: Accelerators, Spectrometers, Detectors and Associated Equipment*, 623(1):276–278, November 2010.

[72] K. Abe et al. Development of low radioactivity photomultiplier tubes for the XMASS-I detector. *Nuclear Instruments and Methods in Physics Research Section A: Accelerators, Spectrometers, Detectors and Associated Equipment*, 922:171–176, April 2019.

[73] XENON Collaboration et al. Lowering the radioactivity of the photomultiplier tubes for the XENON1T dark matter experiment. *Eur. Phys. J. C*, 75(11):546, November 2015.

[74] P. Agnes et al. The electronics, trigger and data acquisition system for the liquid argon time projection chamber of the DarkSide-50 search for dark matter. *J. Inst.*, 12(12):P12011, December 2017.

[75] D. Renker. Geiger-mode avalanche photodiodes, history, properties and problems. *Nucl. Instrum. Meth. A*, 567(1):48–56, 2006.
[76] L. Baudis et al. Characterisation of Silicon Photomultipliers for liquid xenon detectors. *J. Inst.*, 13(10):P10022, October 2018.
[77] A. M. Baldini et al. The design of the MEG II experiment: MEG II Collaboration. *Eur. Phys. J. C*, 78(5):380, May 2018.
[78] B. Abi et al. Volume I. Introduction to DUNE. *J. Inst.*, 15(08):T08008, August 2020.
[79] G. Adhikari et al. nEXO: Neutrinoless double beta decay search beyond 10^{28} year half-life sensitivity. *J. Phys. G: Nucl. Part. Phys.*, 49(1):015104, January 2022.
[80] A. Gola et al. NUV-Sensitive Silicon Photomultiplier Technologies Developed at Fondazione Bruno Kessler. *Sensors*, 19(2):308, January 2019.
[81] T. Pershing et al. Performance of Hamamatsu VUV4 SiPMs for detecting liquid argon scintillation. *JINST*, 17(04):P04017, April 2022.
[82] G. Gallina et al. Performance of novel VUV-sensitive Silicon Photo-Multipliers for nEXO. *Eur. Phys. J. C*, 82(12):1125, December 2022.
[83] G. Collazuol et al. Studies of silicon photomultipliers at cryogenic temperatures. *Nuclear Instruments and Methods in Physics Research Section A: Accelerators, Spectrometers, Detectors and Associated Equipment*, 628(1):389–392, February 2011.
[84] F. Acerbi et al. NUV and VUV sensitive Silicon Photomultipliers technologies optimized for operation at cryogenic temperatures. *Nucl. Instrum. Meth. A*, 1046:167683, November 2022.
[85] T. Wang et al. Characterization of two SiPM arrays from Hamamatsu and Onsemi for liquid argon detector. *Nucl. Instrum. Meth. A*, 1053:168359, May 2023.
[86] M. Capasso et al. FBK VUV-sensitive Silicon Photomultipliers for cryogenic temperatures. *Nucl. Instrum. Meth. A*, 982:164478, December 2020.
[87] Y. Tao et al. Advanced antireflection for back-illuminated silicon photomultipliers to detect faint light. *Sci Rep*, 12(1):13906, August 2022.
[88] P. Jerram et al. Back-thinned CMOS sensor optimization. In S. Jiang et al., editors, *OPTO*, pp. 759813, San Francisco, California, February 2010.
[89] J. Heymes et al. Comparison of Back-Thinned Detector Ultraviolet Quantum Efficiency for Two Commercially Available Passivation Treatments. *IEEE Trans. Nucl. Sci.*, 67(8):1962–1967, August 2020.
[90] A. Razeto et al. Very large SiPM arrays with aggregated output. *JINST*, 17(05):P05038, May 2022.
[91] M. D'Incecco et al. Development of a Very Low-Noise Cryogenic Preamplifier for Large-Area SiPM Devices. *IEEE Trans. Nucl. Sci.*, 65(4):1005–1011, April 2018.
[92] G. Matteucci. Light readout in DarkSide-20k with cryogenic SiPMs. In *11th Symposium on Large TPCs for Low-Energy Rare Event Detection*, December 2023.
[93] T. Frach et al. The digital silicon photomultiplier - Principle of operation and intrinsic detector performance. In *2009 IEEE Nuclear Science Symposium Conference Record (NSS/MIC)*, pp. 1959–1965, Orlando, FL, October 2009. IEEE.
[94] Y. Haemisch et al. Fully Digital Arrays of Silicon Photomultipliers (dSiPM) – a Scalable Alternative to Vacuum Photomultiplier Tubes (PMT). *Physics Procedia*, 37:1546–1560, 2012.
[95] J.-F. Pratte et al. 3D Photon-To-Digital Converter for Radiation Instrumentation: Motivation and Future Works. *Sensors*, 21(2):598, January 2021.
[96] S. Mandai and E. Charbon. Multi-channel digital SiPMs: Concept, analysis and implementation. In *2012 IEEE Nuclear Science Symposium and Medical Imaging Conference Record (NSS/MIC)*, pp. 1840–1844, Anaheim, CA, USA, October 2012. IEEE.
[97] F. Vachon et al. Measuring count rates free from correlated noise in digital silicon photomultipliers. *Meas. Sci. Technol.*, 32(2):025105, February 2021.
[98] L. Parellada-Monreal et al. 3D integration technologies for custom SiPM: From BSI to TSV interconnections. *Nuclear Instruments and Methods in Physics Research Section A: Accelerators, Spectrometers, Detectors and Associated Equipment*, 1049:168042, April 2023.
[99] R. Kugathasan. Integrated front-end electronics for single photon time-stamping in cryogenic dark matter detectors. *J. Inst.*, 15(05):C05019, May 2020.
[100] J. R. Graybill et al. Extreme ultraviolet photon conversion efficiency of tetraphenyl butadiene. *Appl. Opt.*, 59(4):1217, February 2020.
[101] V. Kumar and A. K. Datta. Vacuum ultraviolet scintillators: Sodium salicylate and p-terphenyl. *Appl. Opt.*, 18(9):1414, May 1979.
[102] M. Kuźniak et al. Polyethylene naphthalate film as a wavelength shifter in liquid argon detectors. *Eur. Phys. J. C*, 79(4):291, April 2019.
[103] L. Baudis et al. Enhancement of light yield and stability of radio-pure tetraphenyl-butadiene based coatings for VUV light detection in cryogenic environments. *J. Inst.*, 10(09):P09009–P09009, September 2015.
[104] H. Yang et al. Spin coating of TPB film on acrylic substrate and measurement of its wavelength shifting efficiency. *Nucl. Sci. Tech.*, 31(3):28, March 2020.
[105] B. Abi et al. Volume IV. The DUNE far detector single-phase technology. *J. Inst.*, 15(08):T08010, August 2020.
[106] P. Peiffer et al. Pulse shape analysis of scintillation signals from pure and xenon-doped liquid argon for radioactive background identification. *J. Inst.*, 3(08):P08007, August 2008.
[107] C. G. Wahl et al. Pulse-shape discrimination and energy resolution of a liquid-argon scintillator with xenon doping. *JINST*, 9(06):P06013, 2014.
[108] C. Vogl et al. Scintillation and optical properties of xenon-doped liquid argon. *J. Inst.*, 17(01):C01031, January 2022.
[109] N. Gallice. Xenon doping of liquid argon in ProtoDUNE single phase. *J. Inst.*, 17(01):C01034, January 2022.
[110] J. Soto-Oton. Impact of xenon doping in the scintillation light in a large liquid-argon TPC. *J. Phys.: Conf. Ser.*, 2374(1):012164, November 2022.
[111] DUNE Collaboration et al. Doping Liquid Argon with Xenon in ProtoDUNE Single-Phase: Effects on Scintillation Light, February 2024.
[112] M. Kuźniak and A. M. Szelc. Wavelength Shifters for Applications in Liquid Argon Detectors. *Instruments*, 5(1):4, December 2020.
[113] R. Ajaj et al. Search for dark matter with a 231-day exposure of liquid argon using DEAP-3600 at SNOLAB. *Phys. Rev. D*, 100(2):022004, July 2019.
[114] J. Aalbers et al. First Dark Matter Search Results from the LUX-ZEPLIN (LZ) Experiment. *Phys. Rev. Lett.*, 131(4):041002, July 2023.
[115] E. Aprile et al. First Dark Matter Search with Nuclear Recoils from the XENONnT Experiment. *Phys. Rev. Lett.*, 131(4):041003, July 2023.
[116] E. Aprile et al. Search for Coherent Elastic Scattering of Solar B 8 Neutrinos in the XENON1T Dark Matter Experiment. *Phys. Rev. Lett.*, 126(9):091301, March 2021.
[117] Q. Wang et al. Results of dark matter search using the full PandaX-II exposure. *Chinese Phys. C*, 44(12):125001, December 2020.
[118] A. H. Abdelhameed et al. First results from the CRESST-III low-mass dark matter program. *Phys. Rev. D*, 100(10):102002, November 2019.
[119] J. Aalbers et al. DARWIN: Towards the ultimate dark matter detector. *J. Cosmol. Astropart. Phys.*, 2016(11):017, November 2016.
[120] J. Aalbers et al. A next-generation liquid xenon observatory for dark matter and neutrino physics. *J. Phys. G*, 50(1):013001, December 2022.
[121] LNGS. The Darkside Experiment. https://www.lngs.infn.it/it/darkside.
[122] DEAP3600 Collaboration. DEAP3600 Official Website. https://deap3600.ca/, November 2018.

[123] P. Adhikari et al. First Direct Detection Constraints on Planck-Scale Mass Dark Matter with Multiple-Scatter Signatures Using the DEAP-3600 Detector. *Phys. Rev. Lett.*, 128(1):011801, January 2022.
[124] P. Adhikari et al. The liquid-argon scintillation pulseshape in DEAP-3600. *Eur. Phys. J. C*, 80(4):303, April 2020.
[125] P. Adhikari et al. Precision measurement of the specific activity of ^{39}Ar in atmospheric argon with the DEAP-3600 detector. *Eur. Phys. J. C*, 83(7):642, July 2023.
[126] I. Manthos. DarkSide-20k: Next generation Direct Dark Matter searches with liquid Argon. *arXiv*, 2312.03597, December 2023.
[127] DarkSide-20k Collaboration et al. DarkSide-20k sensitivity to light dark matter particles, July 2024.
[128] D. Montanari et al. Development of membrane cryostats for large liquid argon neutrino detectors. *IOP Conf. Ser.: Mater. Sci. Eng.*, 101:012049, December 2015.
[129] B. Abi et al. The Single-Phase ProtoDUNE Technical Design Report. *arXiv*, 2203.08084, 2017.
[130] DarkSide-20k Collaboration et al. A new hybrid gadolinium nanoparticles-loaded polymeric material for neutron detection in rare event searches, April 2024.
[131] P. Agnes et al. Separating 39Ar from 40Ar by cryogenic distillation with Aria for dark matter searches. *Eur. Phys. J. C*, 81(4):359, April 2021.
[132] E. Aaron et al. Measurement of isotopic separation of argon with the prototype of the cryogenic distillation plant Aria for dark matter searches. *Eur. Phys. J. C*, 83(5):453, May 2023.
[133] C. Aalseth et al. Design and construction of a new detector to measure ultra-low radioactive-isotope contamination of argon. *JINST*, 15(02):P02024, February 2020.
[134] A. Elersich et al. Study of cosmogenic activation above ground for the DarkSide-20k experiment. *Astropart. Phys.*, 152:102878, June 2023.
[135] D. S. Akerib et al. Snowmass2021 Cosmic Frontier Dark Matter Direct Detection to the Neutrino Fog. *arXiv*, 2203.08084, 2022.
[136] G. K. Giovanetti and GADMC. Searching for Dark Matter with Liquid Argon - Snowmass 2021, 2021.
[137] N. Grevesse and A. Sauval. Standard Solar Composition. *Space Science Reviews*, 85(1/2):161–174, 1998.
[138] M. Asplund et al. The Chemical Composition of the Sun. *Annu. Rev. Astron. Astrophys.*, 47(1):481–522, September 2009.
[139] P. Agnes et al. Sensitivity of future liquid argon dark matter search experiments to core-collapse supernova neutrinos. *J. Cosmol. Astropart. Phys.*, 2021(03):043, March 2021.
[140] DUNE Collaboration et al. The DUNE Far Detector Vertical Drift Technology, Technical Design Report. *arXiv*, 2312.03130, 2023.
[141] A. Machado et al. The X-ARAPUCA: An improvement of the ARAPUCA device. *J. Inst.*, 13(04):C04026, April 2018.
[142] 2023 Particle Physics Project Prioritization Panel. Exploring the Quantum Universe. Pathways to Innovation and Discovery in Particle Physics, P5, 2023.
[143] W. T. Chen et al. Flat optics with dispersion-engineered metasurfaces. *Nat Rev Mater*, 5(8):604–620, June 2020.
[144] A. L. Villalpando et al. Improving the light collection efficiency of silicon photomultipliers through the use of metalenses. *J. Inst.*, 15(11):P11021, November 2020.
[145] D. Nygren and Y. Mei. Q-Pix: Pixel-scale Signal Capture for Kiloton Liquid Argon TPC Detectors: Time-to-Charge Waveform Capture, Local Clocks, Dynamic Networks. *arXiv*, 1809.10213, 2018.
[146] P. Miao et al. Demonstrating the Q-Pix front-end using discrete OpAmp and CMOS transistors. *arXiv*, 2311.09568, 2023.
[147] D. Dwyer et al. LArPix: Demonstration of low-power 3D pixelated charge readout for liquid argon time projection chambers. *J. Inst.*, 13(10):P10007, October 2018.
[148] S. Parsa et al. SoLAr: Solar Neutrinos in Liquid Argon. *arXiv*, 2203.07501, 2022.
[149] E. Gramellini. Thin A-Se films for novel scintillation light detectors. In *CPAD Instrumentation Frontier Workshop 2021*, March 2021.
[150] M. Rooks et al. Development of a novel, windowless, amorphous selenium based photodetector for use in liquid noble detectors. *J. Inst.*, 18(01):P01029, January 2023.
[151] D. Y. Akimov et al. Two-phase xenon emission detector with electron multiplier and optical readout by multipixel avalanche Geiger photodiodes. *J. Inst.*, 8(05):P05017, May 2013.
[152] A. Bondar et al. First demonstration of THGEM/GAPD-matrix optical readout in a two-phase Cryogenic Avalanche Detector in Ar. *Nuclear Instruments and Methods in Physics Research Section A: Accelerators, Spectrometers, Detectors and Associated Equipment*, 732:213–216, December 2013.
[153] D. Hollywood et al. ARIADNE—A novel optical LArTPC: Technical design report and initial characterisation using a secondary beam from the CERN PS and cosmic muons. *J. Inst.*, 15(03):P03003, March 2020.
[154] A. J. Lowe et al. ARIADNE+: Large Scale Demonstration of Fast Optical Readout for Dual-Phase LArTPCs at the CERN Neutrino Platform. In *NuFACT 2022*, pp. 46. MDPI, August 2023.
[155] T. Poikela et al. Timepix3: A 65K channel hybrid pixel readout chip with simultaneous ToA/ToT and sparse readout. *J. Inst.*, 9(05):C05013, May 2014.
[156] X. Llopart et al. Timepix4, a large area pixel detector readout chip which can be tiled on 4 sides providing sub-200 ps timestamp binning. *J. Inst.*, 17(01):C01044, January 2022.
[157] A. Breskin. Liquid Hole-Multipliers: A potential concept for large single-phase noble-liquid TPCs of rare events. *J. Phys.: Conf. Ser.*, 460:012020, October 2013.
[158] E. Erdal et al. Recent advances in bubble-assisted Liquid Hole-Multipliers in liquid xenon. *J. Inst.*, 13(12):P12008, December 2018.
[159] E. Erdal et al. Bubble-assisted Liquid Hole Multipliers in LXe and LAr: Towards "local dual-phase TPCs". *J. Inst.*, 15(04):C04002, April 2020.
[160] L. Necib et al. Boosted dark matter at neutrino experiments. *Phys. Rev. D*, 95(7):075018, April 2017.
[161] J. Berger et al. Snowmass 2021 White Paper: Cosmogenic Dark Matter and Exotic Particle Searches in Neutrino Experiments. *arXiv*, 2207.02882, 2022.
[162] A. Abed Abud et al. Snowmass Neutrino Frontier: DUNE Physics Summary. *arXiv*, 2203.06100, 2022.
[163] A. Mastbaum et al. Xenon-doped liquid argon TPCs as a neutrinoless double beta decay platform. *Phys. Rev. D*, 106(9):092002, November 2022.